SALUBI, V., MAHON, R. and OLUYEMI, G. 2022. The combined effect of fluid rheology, inner pipe rotation and eccentricity on the flow of Newtonian and non-Newtonian fluid through the annuli. *Journal of petroleum science and engineering* [online], 211, article 110018. Available from: https://doi.org/10.1016/j.petrol.2021.110018

# The combined effect of fluid rheology, inner pipe rotation and eccentricity on the flow of Newtonian and non-Newtonian fluid through the annuli.

SALUBI, V., MAHON, R. and OLUYEMI, G.

2022

OpenAIR @RGU

This document was downloaded from https://openair.rgu.ac.uk

CC BY NC ND

# The Combined Effect of Fluid Rheology, Inner Pipe Rotation and Eccentricity on the Flow of Newtonian and non-Newtonian Fluid Through the Annuli

Voke Salubi[*], Ruissein Mahon, Gbenga Oluyemi
[a]School of Engineering, Robert Gordon University, Aberdeen, UK, AB10 7GJ
*Email: v.salubi@rgu.ac.uk (V. Salubi), r.r.mahon@rgu.ac.uk (R. Mahon)

## Abstract

The accurate prediction of the fluid dynamics and hydraulics of the axial or helical flow of non-Newtonian drilling fluids in the annuli is essential for the determination and effective management of wellbore pressure during drilling operations. Previous studies have shown that the pressure losses and fluid velocity distributions in the annuli are highly influenced by the rheological properties of the fluid, inner pipe rotary speed and eccentricity. However, many studies in literature have developed or applied theoretical models that were either only valid for Newtonian annuli flows or have not considered the combined effect of the fluid rheological parameters with the inner pipe rotary speed and eccentricity when calculating the frictional annuli pressure losses for non-Newtonian shear thinning fluids. Furthermore, there have been inconsistencies in the description of the effect of inner pipe rotation on the pressure losses experienced for both Newtonian and non-Newtonian flows in concentric and eccentric annuli. In this study, an analytical and numerical approach were carried out to investigate and evaluate the hydrodynamic behaviour of the axial and helical isothermal flow of Newtonian and non-Newtonian fluids through the annuli. Techniques of computational fluid dynamics for fully developed steady-state fluid flow were applied to obtain detailed information of the flow field in the annuli. New analytical and numerical models were developed to obtain the fluid velocity and viscosity field distribution and determine the frictional pressure gradient for laminar and turbulent flows in the concentric and eccentric annuli with and without inner pipe rotation and were compared and validated favourably with models previously presented in literature. Results showed that for a fully developed flow of non-Newtonian shear thinning fluids, if the fluid flowrate is kept constant, an increase in inner pipe rotation leads to a decrease in the axial frictional pressure gradient when the pipe is rotating on its axis. For annuli flows of non-Newtonian fluids, the effect of inner pipe rotation on the axial pressure gradient is dependent on the fluid flowrate and at high fluid flowrates, the influence of the inner pipe rotation on the fluid hydraulics decreases. In general, for shear thinning non-Newtonian fluids, pipe rotation can improve the fluid flow in the region of lower flow in the eccentric annuli. Unlike the flow of Newtonian fluids through the annuli, the friction geometry parameter and thus the friction factor is highly influenced by the rheological parameters of the fluid, the fluid flowrate, inner pipe rotary speed and eccentricity.

**Keywords:** Drilling hydraulics, Friction factor, Inner pipe rotation, Eccentricity, Axial pressure losses, Newtonian, Non-Newtonian

## Highlights

- Friction geometry parameter is dependent on fluid rheology and pipe rotation.
- Inner pipe rotation influences axial velocity fields in the eccentric annuli.
- Eccentricity leads to a decrease in frictional pressure losses.

## 1.0 Introduction

The prediction of the pressure losses for helical flow in the concentric and eccentric annuli is required in order to achieve an effective wellbore pressure management system during drilling operations. Several studies have reported that the variations in the wellbore eccentricity, fluid rheology, annular geometry and drillpipe rotation speed strongly influences the pressure gradient for fluid flow through the annuli. However, there is no rigorous method available to perform annuli flow hydraulic calculations for non-Newtonian fluids, while simultaneously accounting for the combined effect of the important and influential drilling parameters. Although field and laboratory results have shown that the pressure losses in the wellbore can be significantly affected by the rotation of the drillpipe (Ahmed and Miska, 2008), the effects of the drillpipe rotation is usually not taken into consideration when performing predictive calculations (Hemphill, 2015). Furthermore, for helical flow of Newtonian and non-Newtonian fluids through the annuli, the knowledge of the effect of the inner pipe rotation on the frictional pressure gradient has not been conclusively agreed upon in literature. For instance, while some studies reported that the increase in the inner pipe rotation speed increases the pressure gradient, others have reported that the annuli pressure gradient decreases with an increase in the inner pipe rotation speed. Thus, the actual effect of drillpipe rotation on wellbore hydraulics is to an extent not a certitude.

In a study performed by Kelessidis et al. (2006), it was concluded that the accurate prediction of the distribution of the velocity fields and pressure drop for fluid flow through the annulus can be significantly affected by the rheological parameters of the drilling fluid. They showed that the impact of the model can be significant for pressure loss estimation for the flow of non-Newtonian fluids in drill pipes and concentric annuli. McCann et al. (1995) carried out a study to investigate the effects of pipe rotation, fluid properties and eccentricity on the pressure loss for flow of fluids through the annuli. Experimental tests were performed with a maximum pipe rotation speed of 900 rpm, a maximum flowrate of 12 gpm and conclusions were drawn that the pressure loss decreases with an increase in the pipe rotation speed for laminar flow conditions and increased with an increase in the pipe rotation speed for the turbulent flow conditions. They compared their results to hydraulic friction factor models from literature and reported a favourable match for conditions without pipe rotation. However, since the hydraulic models did not account for the effects of eccentricity and pipe rotation, they recommended that hydraulic models should be developed to accurately determine the pressure losses for laminar and turbulent flow in the concentric and eccentric annuli with pipe rotation. Nouri et al. (1997) performed an experimental study of the effect of pipe rotation on Newtonian and non-Newtonian fluid flow through the concentric and eccentric annulus and concluded that the flow resistance increased with an increase in pipe rotation by more than 30% at the lowest Reynolds number but at the higher Reynolds number, the flow resistance was largely unaffected. Wei et al. (1998) investigated the effects of drillpipe rotation on the frictional pressure losses for laminar, helical flow of Power law fluids through a theoretical study and developed flow models for concentric and eccentric pipe configurations with the assumption that the pipe rotates about its axis. They concluded that the shear-thinning effect induced by pipe rotation results in a reduction of the frictional pressure loss in both concentric and eccentric annuli configurations. However, they reported that the effect of the pressure reduction was more pronounced in the concentric annuli. Ooms et al. (1999) carried out a numerical, analytical and experimental study to investigate the influence of drillpipe rotation on drilling hydraulics and concluded that for laminar flow through an eccentric annulus, the inertial effect induced by the pipe rotation increases the axial pressure drop. They inferred that the magnitude of this increase was dependent on the annular gap width, the eccentricity, and the Taylor number of the flow. Sunthankar et al. (2003) in an experimental study of the flow of an aerated mud though an inclined annulus, reported that drillpipe rotation had no significant effect on the pressure losses for air-water fluid mixtures. However, they reported that the pressure losses experienced by the flow of air-aqueous polymer decreased with an increase in the drillpipe rotation and a more significant pressure loss was experienced by the of air-aqueous polymer fluid flows in comparison to that of the air-water fluids. Pereira et al. (2007) performed numerical computational fluid dynamics (CFD) simulations to study the flow of non-Newtonian fluids through a horizontal concentric and eccentric annulus. They reported a decrease in the pressure loss with an increase in the pipe rotation for both the concentric and eccentric annulus. However, it was mentioned that the effect of pipe rotation was more significant at lower fluid flowrates and that reduction of the pressure loss with rotation was more evident in the eccentric cases than the concentric cases. Ahmed and Miska (2008) theoretically and experimentally investigated the laminar flow of Herschel-Buckley fluids in the concentric and eccentric annuli with inner pipe rotation. They compared the model predicted to the experimentally measured pressure losses and concluded that for the flow of shear thinning fluids in highly eccentric annuli, the inertial effects dominate the effect of shear thinning which results in an increase in the annuli pressure loss with an increase in inner pipe rotation. However, the theoretical model developed was only valid for concentric annuli flow of non-Newtonian fluids. Duan et al. (2008) pointed out that inner pipe rotation influences the velocity distribution and axial pressure drop in the annulus. They concluded that an increase in drillpipe rotation slightly increased the pressure drop in the concentric annuli. Ozbayoglu and Sorgun (2009) investigated the effects of pipe rotation on the frictional pressure losses experienced by the flow of non-Newtonian fluids in the annuli. They reported that an increase in the pipe rotational speed led to a corresponding increase in the frictional pressure losses in the annuli and that after a certain pipe rotation speed, there is no influence of the pipe rotation on the pressure loss. They suggested the use of friction factors equations that are functions of the axial and rotational Reynolds number for the calculation of pressure losses in the annuli. Bui (2012) in an attempt to investigate the effect of tool joint and pipe rotation on pressure loss performed numerical CFD simulations for the flow of an incompressible Yield Power Law fluid in both pipe and concentric and eccentric annuli at different pipe rotary speeds. They analysed the numerical results of their velocity and pressure profiles and reported that they observed an increase in pressure drop at low pipe rotary speeds followed by a decrease in pressure drop as the pipe rotary speed was increase. Erge et al. (2014a, 2014b) carried out an analysis of the results of their theoretical model prediction and experimental data and concluded that for the flow of Yield Power Law fluids through the annuli, the frictional pressure losses can either increase or decrease with an increase in the drillpipe rotary speed. They pointed out that for turbulent flows, the effect of the drillpipe rotation is insignificant and also stated that the reason most field measurements show an increase in the annuli pressure losses is because of dominant inertial effects. Viera et al. (2014) presented results obtained from an experimental and numerical CFD simulation for the pressure drop of non-Newtonian aqueous solutions of xanthan gum (XG) and carboxymethylcellulose (CMC) fluid flow through a concentric and eccentric annulus. Their results showed that for a concentric annulus, the pressure drop was slightly reduced with an increase in pipe rotation speed. However, the reverse effect of inner pipe rotation was reported to take place in the eccentric annulus where an increase in pressure drop occurred with inner pipe rotation of up to 200 rpm. In a CFD study which examined the effects of drillpipe rotation on cuttings transport in complex wellbores, Sun et al. (2014) concluded that the increase in pipe rotation can significantly increase the tangential velocity of the drilling fluid and at low and medium flowrates, can significantly reduce the cuttings volume and decrease the pressure loss in the annuli. Bicalho et al. (2016) performed CFD simulations and experimental studies to analyse the pressure gradient and velocity distribution for the flow of various concentrations of aqueous XG solutions through a partially obstructed annulus, with or without inner cylinder rotation. They mentioned that for the fluid with 0.5% of XG, a decrease in the pressure loss with an increase in the inner pipe rotation was observed. Ferroudji et al. (2021) studied the influence of inner pipe orbital motion on the frictional pressure drop for the annuli flow of non-Newtonian fluids under the laminar and turbulent flow regimes. They reported that their results showed that the impact of the orbital motion on the frictional pressure drop of the inner pipe was dependent on the Reynolds number of the flow. However, they concluded that eccentricity decreases the pressure drop and although the increase in orbital motion is severe on the frictional pressure loss, there is a certain speed after which the frictional pressure loss starts to decrease due to the shear thinning properties of the fluid

Although many other studies been done to investigate the effect of pipe rotation and eccentricity on the pressure loss for flow through the annuli (Ahmed et al., 2010; Escudier et al., 2002; Podryabinkin et al., 2013; Saasen, 2014), it is quite clear that the effect of inner pipe rotation on the annuli pressure loss has been quite conflicting. While some studies have reported a decrease in annuli pressure loss due to pipe rotation, others have reported an increase or both an increase and decrease in annuli pressure due to pipe rotation. Although pipe rotation has been reported in many studies to significantly improve cuttings transport (Busch and Johansen, 2020; Erge and van Oort, 2020; Huque et al., 2020; Peden et al., 1990; Sanchez et al., 1999) the prediction of the direct effect of the pipe rotation on the concentric or eccentric annuli pressure loss is highly required to control and maintain wellbore pressures. Caetano et al. (1992) presented friction factor equations for axial steady-state annuli flows, expressed as a function of the annuli friction geometry parameter and determined from the solution of the continuity equation, equation of motion and the Fanning equation. Although these equations were derived for fully developed Newtonian annuli flows, some studies have applied them when mathematically modelling non-Newtonian annuli flows (Ibarra et al., 2019; Lage and Time, 2002). However, the Caetano et al. (1992) friction factors equations cannot be applied to address the effect of the inner pipe rotation on non-Newtonian annuli fluid flows. Over the years, many mathematical modelling performed for single-phase and two-phase fluid flow in the annuli, have either applied friction factor equations valid for Newtonian annuli flows when dealing with Newtonian fluids, or have applied Newtonian or non-Newtonian friction factor equations that have not taken into consideration the combined effect of the fluid rheology, the eccentricity and the effect of the inner pipe rotation when dealing with non-Newtonian fluid flow through the annuli (Fan et al., 2009; Hasan and Kabir, 1992; Kelessidis and Dukler, 1989; Metin and Ozbayoglu, 2009; Omurlu and Ozbayoglu, 2006). Due to the complexity of the solution of non-Newtonian flow in the eccentric annuli, early theoretical methods where the annulus is modelled as a slit of variable height, by an infinite number of concentric annuli with variable outer radii, or by expressing the annuli in the bi-polar coordinate system in order to derive equations for the velocity profiles and pressure gradient to flowrate relationships (Haciislamoglu and Langlinais, 1990; Iyoho and Azar, 1981; Luo and Peden, 1990; Uner et al., 1988). Thus, a rigorous treatment of the annuli flow field is possible to develop hydraulic models that can be applied to predict the pressure losses for flow of non-Newtonian fluids in the concentric and eccentric annuli with inner pipe rotation. In order to establish a relaible method that can be applied to predict the pressure loss for the flow non-Newtonain flows through the annuli with or without inner pipe rotation, it is important that the combined effect of the flow geometric sizes, pipe diameter ratio, eccentricity and importantly the rheological charascteristic and paramters of the fluids be adequately taken into account. The direct application of methods developed for the annuli flow of Newtonian fluids or non-Newtonian fluids that neglects one or more of these important parmaters may generate erroneous results.

In this study, the combined effect of the eccentricity and inner pipe rotation on the flow dynamics and hydraulics of Newtonian and shear thinning non-Newtonian fluid flow through the annuli was investigated. The motivation of this work was to establish new methods that can be applied to obtain the relevant details of the flow fields and predict the pressure gradient for the flow of Newtonian, Power law, Bingham plastic and Herschel-Bulkley fluids in the concentric and eccentric annuli with or without inner pipe rotation, thereby providing a solution to the conflicting issues about the hydraulics of helical flows present in literature.

New analytical and numerical models were developed for the prediction of the friction geometry parameter and frictional presure gradient in the annuli for axial and helical flows of both Newtonian and non-Newtonian fluids in the concentric and eccentric annuli. The newly presented analytical models can be applied to predict the friction factor for both laminar and tubulent flows in the concentric and eccentric annuli, with or without inner pipe rotation. The output of this study provides valuable findings that can be applied to achieve an effective wellbore pressure management system during drilling as well as other industries where there are operations involving annular flows.

## 2.0 Analytical model development

### 2.1 Fluid rheology model

A general fluid rheology model that can be used to describe the shear stress to shear rate relationship for the flow of Newtonian, Power law, Bingham plastic and Herschel-Bulkley fluids is expressed as:

$$\tau = \tau_{\in} + \in \gamma^{n} \qquad \text{(Eq.1)}$$

The viscosity or apparent viscosity of the fluids may then be expressed as:

$$\mu_a = \frac{\tau_{\in}}{\gamma} + \in \gamma^{n-1} \qquad \text{(Eq.2)}$$

The variables $\tau_{\in}$, $\in$, and n are the yield stress, consistency index, and flow behaviour index of the drilling fluid. Table 1 shows the rheology model input constants for both the Newtonian and non-Newtonian fluids.

Table 1:Variables for the generalised rheology model

| **Fluid rheology type** | $\tau_{\in}$ | $\in$ | n |
|---|---|---|---|
| Newtonian | $\tau_{\in} = 0$ | $\in = \mu$ | $n = 1$ |
| Power law (shear thinning) | $\tau_{\in} = 0$ | $\in = K$ | $n < 1$ |
| Bingham plastic | $\tau_{\in} = \tau_y$ | $\in = \mu_p$ | $n = 1$ |
| Herschel-Bulkley (shear thinning) | $\tau_{\in} = \tau_o$ | $\in = K$ | $n < 1$ |

Considering the generalised rheology model of the fluids given in Eq. 1, the generalised Reynolds number for the Newtonian, Power law, Bingham plastic and Herschel-Bulkley fluids can be derived and expressed as follows:

$$Re_{Gen} = \frac{\rho V_a D_h}{\frac{\tau_\epsilon D_h}{12V_a} + \epsilon \left(\frac{2m+1}{3m}\right)^n \left(\frac{12V_a}{D_h}\right)^{n-1}} \quad \text{(Eq.3)}$$

$$m = \frac{n \ \epsilon \ \left(\frac{12V_a}{D_h}\right)^n}{\tau_\epsilon + \epsilon \ \left(\frac{12V_a}{D_h}\right)^n} \quad \text{(Eq.4)}$$

The details of the derivation procedure of Equation 3 and 4 is provided in Appendix C.

**2.2 Helical flow of fluids in the annuli**

When the drillpipe is rotated, the drilling fluid would experience a multi-directional shear force that creates the helical movement of the fluid. Thus, the shear stress to shear rate relationship, which is the fluid rheology model, must be represented in a tensor form. The magnitude of the shear rate for a multi-directional shear flow can be expressed in the cylindrical coordinate system as:

$$|\gamma^2| = 2\left[\left(\frac{\partial v_r}{\partial r}\right)^2 + \left(\frac{1}{r}\frac{\partial v_\theta}{\partial \theta} + \frac{v_r}{r}\right)^2 + \left(\frac{\partial v_z}{\partial z}\right)^2\right] + \left(\frac{1}{r}\frac{\partial v_z}{\partial \theta} + \frac{\partial v_\theta}{\partial z}\right)^2 + \left[\frac{1}{r}\frac{\partial v_r}{\partial \theta} + r\frac{\partial}{\partial r}\left(\frac{v_\theta}{r}\right)\right]^2 + \left(\frac{\partial v_z}{\partial r} + \frac{\partial v_r}{\partial z}\right)^2 \quad \text{(Eq.5)}$$

Unlike the concentric annuli, the velocity distribution of the helical flow in the eccentric annuli varies in the radial and angular directions, making the theoretical solution for the annuli flow of non-Newtonian fluids relatively very complex. Assuming that the flow is fully developed, the governing equations for helical fluid flow in the eccentric annuli can be solved using the same method of that of the concentric annuli. This can be done by applying the concept of an infinite subdivision of the flow field of the helical flow in eccentric annuli (Hai-qiao and Ji-zhou, 1994). Thus, it can be convenient to express the magnitude of the fluid shear rate in the helical concentric and eccentric annuli as:

$$|\gamma| = \sqrt{\left(r\frac{\partial \omega}{\partial r}\right)^2 + \left(\frac{\partial v_z}{\partial r}\right)^2} \quad \text{(Eq.6)}$$

where, $v_\theta = \omega r$

Similarly, the magnitude of the shear stress for the helical flow of fluids can be expressed as:

$$|\tau| = \sqrt{\tau_{zr}^2 + \tau_{\theta r}^2} \quad \text{(Eq.7)}$$

Adopting the form of the Newtonian model, the axial and tangential shear stresses may be expressed in form of their velocity gradients as:

$$\tau_{\theta r} = \mu_a \left(r\frac{\partial \omega}{\partial r}\right) \quad \text{(Eq.8)}$$

$$\tau_{zr} = -\mu_a \left(\frac{\partial v_z}{\partial r}\right) \quad \text{(Eq.9)}$$

Thus, the apparent viscosity of the fluids in the annuli with inner pipe rotation can be expressed as follows:

$$\mu_a = \frac{\tau_\in}{|\gamma|} + \in |\gamma|^{n-1} \quad \text{(Eq.10)}$$

$$\mu_a = \frac{\tau_\in}{\left|\sqrt{\left(r\frac{\partial \omega}{\partial r}\right)^2 + \left(\frac{\partial v_z}{\partial r}\right)^2}\right|} + \in \left|\sqrt{\left(r\frac{\partial \omega}{\partial r}\right)^2 + \left(\frac{\partial v_z}{\partial r}\right)^2}\right|^{n-1} \quad \text{(Eq.11)}$$

Using Equations 8 and 9, the apparent viscosity equation can be further simplified to yield:

$$\mu_a = \left[\frac{\in |{\tau_{\theta r}}^2 + {\tau_{zr}}^2|^{\frac{n-1}{2}}}{1 - \frac{\tau_\in}{|{\tau_{\theta r}}^2 + {\tau_{zr}}^2|^{\frac{1}{2}}}}\right]^s \quad \text{(Eq.12)}$$

where $s = 1/n$

Figure 1 shows the shape of the velocity profile for a fully developed annuli flow of non-Newtonian drilling fluids that possess a yield stress. For fluids with a yield stress to flow through the annuli, the axial pressure force must produce a shear stress that exceeds the yield stress $\tau_\in$. Thus, as the fluid flows through the annuli, there is a region of the fluid that does not shear and the fluid elements in this region, move at the local maximum velocity.

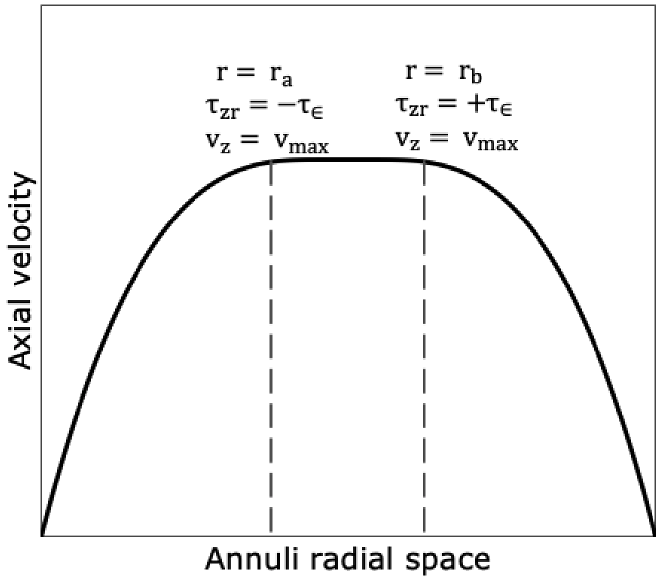


Figure 1: Annuli velocity profile

This unsheared region of the fluid is referred to as the unsheared plug. In the derivation of the shear stress and velocity profiles, the points that mark the boundaries of the unsheared plug in the radial direction are signified as the points $r = r_a$ and $r = r_b$ as shown in Figure 1. For the Herschel-Bulkley drilling fluid the shear stress at point

$r = r_a$ is equal to the negative value of the yield stress $\tau_{zr} = -\tau_{\epsilon} = -\tau_o$ while the shear stress at the point $r = r_b$ is equal to the positive value of the yield stress $\tau_{zr} = +\tau_{\epsilon} = +\tau_o$. Likewise, for the Bingham plastic fluid, the shear stresses at the points $r = r_a$ and $r = r_b$ are equal to the negative and positive value of the Bingham yield stress respectively $\tau_{zr} = -\tau_{\epsilon} = -\tau_y$ and $\tau_{zr} = +\tau_{\epsilon} = +\tau_y$. The Power law fluid does not possess a yield stress and hence does not have the region of an unsheared plug in the annuli. In the axial velocity profile of the Power law fluid, the local maximum velocity exists at the point $r_a = r_b$ and the shear stress at this point is zero $\tau_{zr} = \tau_{\epsilon} = 0$. The width of the unsheared plug can be determined by considering a force balance of the pressure force being equal to the shear force in the region of the plug. The pressure force acts on the cross-sectional area of the plug, while the shear force, which is equal to the yield stress times the surface area of the plug, acts on the inner and outer surfaces of the plug. Performing this force balance over a differential length $\partial z$ of the plug, yields the equation for the width of the plug as:

$$\pi({r_b}^2 - {r_a}^2)\frac{\partial P}{\partial z}\partial z = 2\pi(r_b + r_a)\tau_{\epsilon}\,\partial z \quad \text{(Eq.13)}$$

$$r_b - r_a = \frac{2\tau_{\epsilon}}{\frac{\partial P}{\partial z}} \quad \text{(Eq.14)}$$

$$\tau_{\epsilon} = \frac{1}{2}\frac{\partial P}{\partial z}(r_b - r_a) \quad \text{(Eq.15)}$$

It is obvious that the width of the plug depends on just the axial pressure gradient and the yield stress of the fluid and is independent of the size of the annuli. However, in an eccentric annulus, the width of the unsheared plug and the position of the local maximum velocity varies across the angular direction of the annuli. Thus, the points $r = r_a$ and $r = r_b$ are a function of the angle $\theta$ hence the shear stress and velocity profiles vary across the angular direction of the annuli and are direct functions of the angle $\theta$. To account for this phenomenon, the annuli can be represented by an infinite number of concentric annuli with variable outer radii $r_2^e$ (Luo and Peden, 1990). The outer radius of the eccentric annulus is a function of the angle $\theta$ and the eccentricity e and can be determined with the following equations:

$$r_2^e = d_e \cos\theta + \sqrt{r_2^2 - (d_e \sin\theta)^2} \quad \text{(Eq.16)}$$

$$d_e = (r_2 - r_1)e \quad \text{(Eq.17)}$$

Considering a steady-state isothermal laminar flow of incompressible fluids through the annuli, the governing equations of motion can be integrated to yield the equations for the axial $\tau_{zr}$ and tangential $\tau_{\theta r}$ shear stresses in the cylindrical coordinates as:

$$\tau_{zr} = \frac{\partial P}{\partial z}\frac{r}{2} + \frac{C_z}{r} \quad \text{(Eq.18)}$$

$$\tau_{\theta r} = \frac{C_{\omega}}{r^2} \quad \text{(Eq.19)}$$

The constants $C_z$ and $C_\omega$ in the axial and tangential shear stress equations are constants of integration. The axial shear stress profile at a given angular position in the annuli may be obtained by applying the boundary conditions to Equation 18 that $\tau_{zr} = -\tau_\epsilon$ at $r = r_a$ and inserting Equation 15 to the result to yield:

$$\tau_{zr}(\theta, r) = \frac{1}{2}\frac{\partial P}{\partial z}\left[\left(r - \frac{{r_a}^2}{r}\right) - \frac{r_a(r_b - r_a)}{r}\right] \quad r_1 \le r \le r_a \tag{Eq.20}$$

Similarly, from the boundary condition that $\tau_{zr} = +\tau_\epsilon$ at $r = r_b$, the axial shear stress profile is

$$\tau_{zr}(\theta, r) = \frac{1}{2}\frac{\partial P}{\partial z}\left[\left(r - \frac{{r_b}^2}{r}\right) + \frac{r_b(r_b - r_a)}{r}\right] \quad r_b \le r \le r_2^e \tag{Eq.21}$$

where $r_a = f(\theta, e)$ and $r_b = f(\theta, e)$.

Substituting the axial and tangential shear stress equations into the Equation 12 yields the equation for the annuli viscosity profile as:

$$\mu_a(\theta, r) = \left[\frac{\in \left|\left(\frac{C_\omega}{r^2}\right)^2 + \left(\frac{1}{2}\frac{\partial P}{\partial z}\left[\left(r - \frac{{r_a}^2}{r}\right) - \frac{r_a(r_b - r_a)}{r}\right]\right)^2\right|^{\frac{n-1}{2}}}{1 - \dfrac{\tau_\epsilon}{\left|\left(\frac{C_\omega}{r^2}\right)^2 + \left(\frac{1}{2}\frac{\partial P}{\partial z}\left[\left(r - \frac{{r_a}^2}{r}\right) - \frac{r_a(r_b - r_a)}{r}\right]\right)^2\right|^{\frac{1}{2}}}}\right]^s \tag{Eq.22}$$

Inserting the shear stress profile equations into the Equation 9 and integrating the results with the appropriate boundary conditions produces the velocity profile equation for fluid flow in the concentric and eccentric annulus, with or without drillpipe rotation. In the region of $r_1 \le r \le r_a$, the axial velocity of the fluid increases with an increase in r, so the axial velocity gradient can either be greater than or equal to 0, $\partial v_z/\partial r \ge 0$. Conversely, in the region of $r_b \le r \le r_2^e$, the axial velocity gradient is either zero or a negative value as the fluid velocity decreases with an increase in r. In the region of the maximum axial velocity or the plug region $r_a \le r \le r_b$, the axial velocity gradient is equal to zero $\partial v_z/\partial r = 0$. The velocity gradients or shear rate equations are thereby given as:

$$\frac{\partial v_z}{\partial r} = \frac{1}{2\mu_a(\theta, r)}\frac{\partial P}{\partial z}\left[\left(\frac{{r_a}^2}{r} - r\right) + \frac{r_a(r_b - r_a)}{r}\right] \quad r_1 \le r \le r_a \tag{Eq.23}$$

$$\frac{\partial v_z}{\partial r} = 0 \quad r_a \le r \le r_b \tag{Eq.24}$$

$$\frac{\partial v_z}{\partial r} = \frac{1}{2\mu_a(\theta, r)}\frac{\partial P}{\partial z}\left[\left(r - \frac{{r_b}^2}{r}\right) + \frac{r_b(r_b - r_a)}{r}\right] \quad r_b \le r \le r_2^e \tag{Eq.25}$$

Integrating Equation 23 and applying the no-slip boundary condition that $v_z(\theta, r) = 0$, at the drillpipe wall $r = r_1$ yields the axial velocity profile:

$$v_z(\theta, r) = \frac{1}{2}\frac{\partial P}{\partial z}\int_{r_1}^{r} \frac{1}{\mu_a(\theta, r)}\left[\left(\frac{{r_a}^2}{r} - r\right) + \frac{r_a(r_b - r_a)}{r}\right] dr \quad r_1 \le r \le r_a \qquad \text{(Eq.26)}$$

Similarly, integrating the Equation 25 while applying the no-slip boundary condition that $v_z(\theta, r) = 0$, at the drillpipe wall $r = r_2^e$ yields:

$$v_z(\theta, r) = \frac{1}{2}\frac{\partial P}{\partial z}\int_{r}^{r_2^e} \frac{1}{\mu_a(\theta, r)}\left[\left(r - \frac{{r_b}^2}{r}\right) + \frac{r_b(r_b - r_a)}{r}\right] dr \quad r_b \le r \le r_2^e \qquad \text{(Eq.27)}$$

In the region $r_a \le r \le r_b$, $v_z(\theta, r) = v_z(\theta, r_a) = v_z(\theta, r_b) = v_{zmax}(\theta)$

The angular velocity profile may be derived from Equations 8 and 19 as follows:

$$\frac{\partial \omega}{\partial r} = \frac{1}{\mu_a(\theta, r)}\frac{C_\omega}{r^3} \qquad \text{(Eq.28)}$$

Integrating the above equation and applying the boundary condition that the angular velocity is maximum at the drillpipe wall, $\omega = \omega_{max}$ at $r = r_1$, results in:

$$\omega(\theta, r) = \omega_{max} - C_\omega(\theta, r)\int_{r_1}^{r} \frac{dr}{\mu_a(\theta, r)\, r^3} \qquad \text{(Eq.29)}$$

The volume flow rate for the generalised drilling fluid flow through the concentric and eccentric annulus with or without drillpipe rotation annulus can be expressed by integrating the velocity distribution over the entire annulus region while applying the appropriate boundary conditions:

$$Q = \int_0^{2\pi}\int_{r_1}^{r_2^e} v_z(\theta, r)\, r\, dr d\theta \qquad \text{(Eq.30)}$$

After substituting the equations for the axial velocity profiles into Equation 30, the equation for the volume flow rate of the fluid becomes:

$$Q = \frac{1}{4}\frac{\partial P}{\partial z}\int_0^{2\pi}({r_a}^2 - r^2)\int_{r_1}^{r_a} \frac{1}{\mu_a(\theta, r)}\left[\left(\frac{{r_a}^2}{r} - r\right) + \frac{r_a(r_b - r_a)}{r}\right] dr d\theta$$

$$+ \frac{1}{4}\frac{\partial P}{\partial z}\int_0^{2\pi}({r_a}^2 - {r_b}^2)\int_{r_1}^{r_a} \frac{1}{\mu_a(\theta, r)}\left[\left(\frac{{r_a}^2}{r} - r\right) + \frac{r_a(r_b - r_a)}{r}\right] dr d\theta \qquad \text{(Eq.31)}$$

$$+ \frac{1}{4}\frac{\partial P}{\partial z}\int_0^{2\pi}(r^2 - {r_b}^2)\int_{r_b}^{r_2^e} \frac{1}{\mu_a(\theta, r)}\left[\left(r - \frac{{r_b}^2}{r}\right) + \frac{r_b(r_b - r_a)}{r}\right] dr d\theta$$

The constant $C_\omega(\theta, r)$ can be determined by applying the no-slip boundary condition that $\omega = 0$ at the outer wall of the annulus $r = r_2^e$ , thereby arriving at:

$$C_\omega(\theta, r) = \frac{\omega_{max}}{\int_{r_1}^{r_2^e} \frac{dr}{\mu_a(\theta, r)\, r^3}} \quad \text{(Eq.32)}$$

The following function can be used to determine the radial position $r_a = f(\theta, e)$ and $r_b = f(\theta, e)$.

$$f(r_a, r_b) = \int_{r_1}^{r_a} \frac{1}{\mu_a(\theta, r)} \left[\left(\frac{{r_a}^2}{r} - r\right) + \frac{r_a(r_b - r_a)}{r}\right] dr$$
$$- \int_{r_b}^{r_2^e} \frac{1}{\mu_a(\theta, r)} \left[\left(r - \frac{{r_b}^2}{r}\right) + \frac{r_b(r_b - r_a)}{r}\right] dr \quad \text{(Eq.33)}$$

## 2.3 Friction factor

The Fanning friction factor for a fully developed laminar flow of fluids through the concentric and eccentric annuli with or without inner pipe rotation, may be expressed as a function of the friction geometry parameter $F_\pi$:

$$f = \frac{F_\pi}{Re_{Gen}} \quad \text{(Eq.34)}$$

According to the method suggested by Caetano et al. (1992), the friction factor for turbulent flow in the annuli can be expressed in terms of the friction geometry parameter as:

$$\left\{f\left(\frac{16}{F_\pi}\right)^c\right\}^{-1/2} = 4\log\left\{Re_{Gen}\left(f\left(\frac{16}{F_\pi}\right)^c\right)^{-1/2}\right\} - 0.40 \quad \text{(Eq.35)}$$

where the exponent c in Eq 35 is given as:

$$c = 0.45\exp[-(Re_{Gen} - 3000)/10^6] \quad \text{(Eq.36)}$$

If the friction factor is obtained, the frictional pressure gradient can be determined from the following generally known fluid flow equation:

$$\frac{dP}{dL} = \frac{2f\rho {V_a}^2}{D_h} \quad \text{(Eq.37)}$$

where the hydraulic diameter is given as, $D_h = d_2 - d_1$.

Using the Equations 31, 34 and 37, the friction geometry parameter for the flow of Newtonian and non-Newtonian fluids through the concentric and eccentric annuli, with or without inner pipe rotation can be determined from the solution of the following equations:

$$F_{\pi} = \frac{\pi(d_2 + d_1){D_h}^3}{4S_{\pi}\mu_{Gen}} \tag{Eq.38}$$

$$\mu_{Gen} = \frac{\tau_{\in} D_h}{12V_a} + \in \left(\frac{2m+1}{3m}\right)^n \left(\frac{12V_a}{D_h}\right)^{n-1} \tag{Eq.39}$$

$$\begin{aligned} S_{\pi} = & \int_0^{\pi} ({r_a}^2 - r^2) \int_{r_1}^{r_a} \frac{1}{\mu_a(\theta, r)} \left[\left(\frac{{r_a}^2}{r} - r\right) + \frac{r_a(r_b - r_a)}{r}\right] r dr d\theta \\ & + \int_0^{\pi} ({r_a}^2 - {r_b}^2) \int_{r_1}^{r_a} \frac{1}{\mu_a(\theta, r)} \left[\left(\frac{{r_a}^2}{r} - r\right) + \frac{r_a(r_b - r_a)}{r}\right] r dr d\theta \\ & + \int_0^{\pi} (r^2 - {r_b}^2) \int_{r_b}^{r_2^e} \frac{1}{\mu_a(\theta, r)} \left[\left(r - \frac{{r_b}^2}{r}\right) + \frac{r_b(r_b - r_a)}{r}\right] r dr d\theta \end{aligned} \tag{Eq.40}$$

# 3.0 Numerical model development

## 3.1 Numerical methodology

In order to analyse the steady-state laminar flow of incompressible fluids in the concentric and eccentric annuli with and without inner pipe rotation, a CFD method was applied to discretise and obtain solutions of the governing equations for a fully developed 2D fluid flow. This concept was formulated to enable the execution of steady-state CFD numerical simulations and obtain viscosity fields, axial and tangential velocity fields as well as the provision of data necessary for the evaluation of the fluid flowrate to axial pressure gradient relationship for Newtonian and non-Newtonian fluid flow through the concentric and eccentric annuli, with and without inner pipe rotation. Another benefit of the numerical modelling was the provision of additional data that was used to validate the results obtained from the newly developed analytical models. This involved the development of a numerical simulation technique by applying an unstructured finite volume method where the concentric and eccentric annuli are meshed in a manner that the annuli geometry is comprised of control volumes that are bounded by a finite number of discrete straight edges or planar faces. A triangular mesh for the 2D annuli geometry was generated using a systematic method where each triangular element or control volume has a node at the centroid and vertices of the cells where information of the fluid properties are stored in the annuli geometry. Figure 2 shows the unstructured triangular mesh stencil where one control volume, $i$, is surrounded by three other neighbouring control volumes.

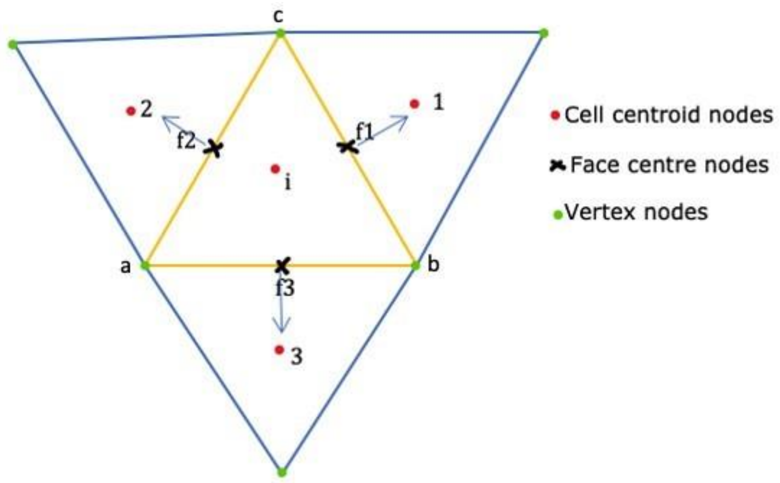


Figure 2:Unstructured mesh control volumes

The momentum equation for an incompressible isothermal flow of a fluid through the annuli is

$$\frac{\partial \mathbf{v}}{\partial t} + \nabla.\mathbf{vv} = -\frac{1}{\rho}\nabla P + \frac{\mu}{\rho}\nabla^2\mathbf{v} + \mathbf{g} \qquad \text{(Eq.41)}$$

Assuming that the flow is at steady-state fully developed and not accelerating, neglecting the gravitational body force, the momentum equation can be simplified to yield:

$$\nabla P = \mu\nabla^2\mathbf{v} \qquad \text{(Eq.42)}$$

To discretise the steady-state momentum equations and obtain solutions for the frictional pressure gradient, the finite volume approach was applied, where the conservation principles of momentum are satisfied at all the centroids of the control volumes in the annuli geometry domain. To integrate the governing equations, the numerical approximation of the diffusion terms in Equation 41 was obtained by defining the average value over a given control volume or cell in the annuli geometry using a volume integral and expressing the volume integral as a surface integral using the Gauss divergence theorem as follows:

$$\nabla^2\mathbf{v} = \frac{1}{V_i}\int_{CV}^{\cdot} \nabla^2\mathbf{v}\ \partial V = \frac{1}{V_i}\int_{CS}^{\cdot} \nabla\mathbf{v}.\mathbf{n}\ \partial A_f \qquad \text{(Eq.43)}$$

From the definition of the volume average, Equation 41 may then be expressed as a summation over the discrete faces bounding a control volume as:

$$\int_{CS}^{\cdot} \nabla\mathbf{v}.\mathbf{n}\ \partial A_f = \sum_{f=1}^{N_{f,i}} \nabla\mathbf{v}_f.\mathbf{n}_f\ A_f = V_i\nabla P \qquad \text{(Eq.44)}$$

Thus, it is assumed that the average value of the pressure gradient over a cell or control volume, $V_i$, is the same as its value at the geometric centroid node of the cell.

$$\int_{CS} \nabla \mathbf{v}.\,\mathbf{n}\ \partial A_f = \sum_{f=1}^{N_{f,i}} \nabla \mathbf{v}_f.\,\mathbf{n}_f\ A_f = V_i \nabla P \qquad \text{(Eq.45)}$$

When the inner pipe is rotating in the annuli, there exists the axial and tangential velocity components in the annuli which is denoted respectively by $v_z$ and $v_\theta$. However, the solution of the equations is not performed using the cylindrical coordinate system and thus, assuming that there is no pressure gradient in the tangential direction, Equation 45 can be expressed as follows:

$$\sum_{f=1}^{N_{f,i}} \nabla v_z.\,\mathbf{n}_f\ A_f = V_i \nabla P \qquad \text{(Eq.46)}$$

$$\sum_{f=1}^{N_{f,i}} \nabla v_\theta.\,\mathbf{n}_f\ A_f = 0 \qquad \text{(Eq.47)}$$

In the annuli geometry, the gradient of the velocity at the faces of the cells were decomposed into vectors in the normal $\mathbf{n}_f$ and tangent $\mathbf{t}_f$ coordinate directions which are mutually perpendicular to each other. In the 2D annuli geometry, it has been assumed that the axial and angular velocities do not vary in the axial direction but varies in the normal and tangential directions. Therefore, the gradient of the axial and tangential velocity fields at the faces bounding the control volume, and in the direction pointing from the centroid of the cell to the centroid of its neighbouring cell across a given face can be written as:

$$(\nabla v_z)_f.\,\mathbf{I}_f = [(\nabla v_z)_f.\,\mathbf{n}_f]\mathbf{n}_f.\,\mathbf{I}_f + [(\nabla v_z)_f.\,\mathbf{t}_f]\mathbf{t}_f.\,\mathbf{I}_f \qquad \text{(Eq.48)}$$

$$(\nabla v_\theta)_f.\,\mathbf{I}_f = [(\nabla v_\theta)_f.\,\mathbf{n}_f]\mathbf{n}_f.\,\mathbf{I}_f + [(\nabla v_\theta)_f.\,\mathbf{t}_f]\mathbf{t}_f.\,\mathbf{I}_f \qquad \text{(Eq.49)}$$

The vector $\mathbf{I}_f$ is the vector pointing from a given cell centre to its neighbouring cell centre across a given face. Thus, the dot product $\mathbf{n}_f.\,\mathbf{I}_f$ is the distance between the cell centre and its neighbouring cell centre and is denoted by $d_f$. Equations 48 and 49 can then be written as:

$$(\nabla v_z)_f.\,\mathbf{n}_f = \frac{(\nabla v_z)_f.\,\mathbf{I}_f}{d_f} - \frac{[(\nabla v_z)_f.\,\mathbf{t}_f]\mathbf{t}_f.\,\mathbf{I}_f}{d_f} \qquad \text{(Eq.50)}$$

$$(\nabla v_\theta)_f.\,\mathbf{n}_f = \frac{(\nabla v_\theta)_f.\,\mathbf{I}_f}{d_f} - \frac{[(\nabla v_\theta)_f.\,\mathbf{t}_f]\mathbf{t}_f.\,\mathbf{I}_f}{d_f} \qquad \text{(Eq.51)}$$

The fluid at the faces of the control volume is subjected to a normal and tangential shear so the viscosity of the fluid at the faces of the cells are calculated from the magnitude of the fluid shear rate as:

$$|\gamma|_f = \sqrt{((\nabla v_z)_f.\,\mathbf{n}_f)^2 + ((\nabla v_z)_f.\,\mathbf{t}_f)^2 + ((\nabla v_\theta)_f.\,\mathbf{n}_f)^2 + 2((\nabla v_\theta)_f.\,\mathbf{t}_f)^2} \qquad \text{(Eq.52)}$$

$$\mu_f = \frac{\tau_\epsilon}{|\gamma|_f} + \epsilon\ |\gamma|_f^{\,n-1} \qquad \text{(Eq.53)}$$

For the cell $i$ in Figure 2, Equations 46 and 47 can be discretised to obtain the following equations for the normal and tangential components in the governing equation.

$$\mu_{f1}\left[\frac{v_{z1}-v_{zi}}{d_{f1}}-\left(\frac{v_{zc}-v_{zb}}{d_{f1}|\mathbf{t}_{f1}|}\right)\mathbf{t}_{f1}.\mathbf{I}_{f1}\right]A_{f1}+\mu_{f2}\left[\frac{v_{z2}-v_{zi}}{d_{f2}}-\left(\frac{v_{za}-v_{zc}}{d_{f2}|\mathbf{t}_{f2}|}\right)\mathbf{t}_{f2}.\mathbf{I}_{f2}\right]A_{f2}$$
$$+\mu_{f3}\left[\frac{v_{z3}-v_{zi}}{d_{f3}}-\left(\frac{v_{zb}-v_{za}}{d_{f3}|\mathbf{t}_{f3}|}\right)\mathbf{t}_{f3}.\mathbf{I}_{f3}\right]A_{f3}=V_i\nabla P \tag{Eq.54}$$

$$\mu_{f1}\left[\frac{v_{\theta 1}-v_{\theta i}}{d_{f1}}-\left(\frac{v_{\theta c}-v_{\theta b}}{d_{f1}|\mathbf{t}_{f1}|}\right)\mathbf{t}_{f1}.\mathbf{I}_{f1}\right]A_{f1}+\mu_{f2}\left[\frac{v_{\theta 2}-v_{\theta i}}{d_{f2}}-\left(\frac{v_{\theta a}-v_{\theta c}}{d_{f2}|\mathbf{t}_{f2}|}\right)\mathbf{t}_{f2}.\mathbf{I}_{f2}\right]A_{f2}$$
$$+\mu_{f3}\left[\frac{v_{\theta 3}-v_{\theta i}}{d_{f3}}-\left(\frac{v_{\theta b}-v_{\theta a}}{d_{f3}|\mathbf{t}_{f3}|}\right)\mathbf{t}_{f3}.\mathbf{I}_{f3}\right]A_{f3}=0 \tag{Eq.55}$$

Equations 54 and 55 can be further simplified to yield the following equations for the axial and tangential velocities that exist at the centroid of all the control volumes in the flow domain.

$$v_{zi}=\frac{\frac{v_{z1}\mu_{f1}}{d_{f1}}A_{f1}+\frac{v_{z2}\mu_{f2}}{d_{f2}}A_{f2}+\frac{v_{z3}\mu_{f3}}{d_{f3}}A_{f3}-\mu_{f1}\left(\frac{v_{zc}-v_{zb}}{d_{f1}|\mathbf{t}_{f1}|}\right)\mathbf{t}_{f1}.\mathbf{I}_{f1}A_{f1}-\mu_{f2}\left(\frac{v_{za}-v_{zc}}{d_{f2}|\mathbf{t}_{f2}|}\right)\mathbf{t}_{f2}.\mathbf{I}_{f2}A_{f2}-\mu_{f3}\left(\frac{v_{zb}-v_{za}}{d_{f3}|\mathbf{t}_{f3}|}\right)\mathbf{t}_{f3}.\mathbf{I}_{f3}A_{f3}-V_i\nabla P}{\frac{\mu_{f1}}{d_{f1}}A_{f1}+\frac{\mu_{f2}}{d_{f2}}A_{f2}+\frac{\mu_{f3}}{d_{f3}}A_{f3}} \tag{Eq.56}$$

$$v_{\theta i}=\frac{\frac{v_{\theta 1}\mu_{f1}}{d_{f1}}A_{f1}+\frac{v_{\theta 2}\mu_{f2}}{d_{f2}}A_{f2}+\frac{v_{\theta 3}\mu_{f3}}{d_{f3}}A_{f3}-\mu_{f1}\left(\frac{v_{\theta c}-v_{\theta b}}{d_{f1}|\mathbf{t}_{f1}|}\right)\mathbf{t}_{f1}.\mathbf{I}_{f1}A_{f1}-\mu_{f2}\left(\frac{v_{\theta a}-v_{\theta c}}{d_{f2}|\mathbf{t}_{f2}|}\right)\mathbf{t}_{f2}.\mathbf{I}_{f2}A_{f2}-\mu_{f3}\left(\frac{v_{\theta b}-v_{\theta a}}{d_{f3}|\mathbf{t}_{f3}|}\right)\mathbf{t}_{f3}.\mathbf{I}_{f3}A_{f3}}{\frac{\mu_{f1}}{d_{f1}}A_{f1}+\frac{\mu_{f2}}{d_{f2}}A_{f2}+\frac{\mu_{f3}}{d_{f3}}A_{f3}} \tag{Eq.57}$$

The velocities at the vertex nodes are computed from interpolation of the velocities in the cells that are in contact with the vertex node. Although there are several ways in which this interpolation can be performed, the interpolation function used for the computation of the vertex velocities is dependent on the distance between the vertex node and the surrounding cell central nodes. The cell-to-vertex interpolation function can be expressed as:

$$v_v=\sum_{i=1}^{N}w_{v,i}\,v_i \tag{Eq.58}$$

$$w_{v,i}=\frac{1/d_i}{\sum_{i=1}^{N}1/d_i} \tag{Eq.59}$$

where $d_i$, is the distance of the ith cell node to the vertex node and N is the number of cells that influences the vertex node.

The area of the faces of the control volume is equal to the length of the face so for instance, considering the face 1 of the cell $i$ in Figure 2, the area of the face can be determined from:

$$A_{f1} = \sqrt{(x_c - x_b)^2 + (y_c - y_b)^2} \quad \text{(Eq.60)}$$

In order to mitigate the numerical precision errors when determining the volume of a cell regardless of the shape or orientation, an average of the volumes is obtained using the two components of the outward unit normal summed over the faces of the control volume. Thus, the volume of a cell in the domain may be expressed as:

$$V_i = \frac{1}{2}\left(\sum_{f=1}^{N_{f,i}} n_{x,f}\, x_f\, A_f + \sum_{f=1}^{N_{f,i}} n_{y,f}\, y_f\, A_f\right) \quad \text{(Eq.61)}$$

where $x_f$, $y_f$ and $z_f$ are the coordinates of the centroid of the faces of the control volume.

## 4.0 Mesh and simulation parameters

Fluid flow simulations were performed to analyse the combined effect of the fluid rheology, eccentricity and inner pipe rotation on the flow dynamics, friction geometry parameter and frictional pressure gradient for annuli flows using the newly developed analytical and numerical CFD models. Table 2 presents the range of the input parameters that were used to perform analytical and numerical CFD simulations.

Table 2: Range of input parameters considered

| Input parameters | Range of values |
|---|---|
| Fluid circulation rate | 10 to 70 $m^3$/hr |
| Inner and outer pipe size | 88 and 144 mm |
| Inner pipe rotary speed | 0 to 320 rpm |
| Eccentricity | 0 to 0.9 |

A computational program was written in MATLAB to obtain solutions for the velocity and viscosity numerical CFD equations.
Figure *3* shows the annuli geometry and mesh generated for the concentric and eccentric annuli.

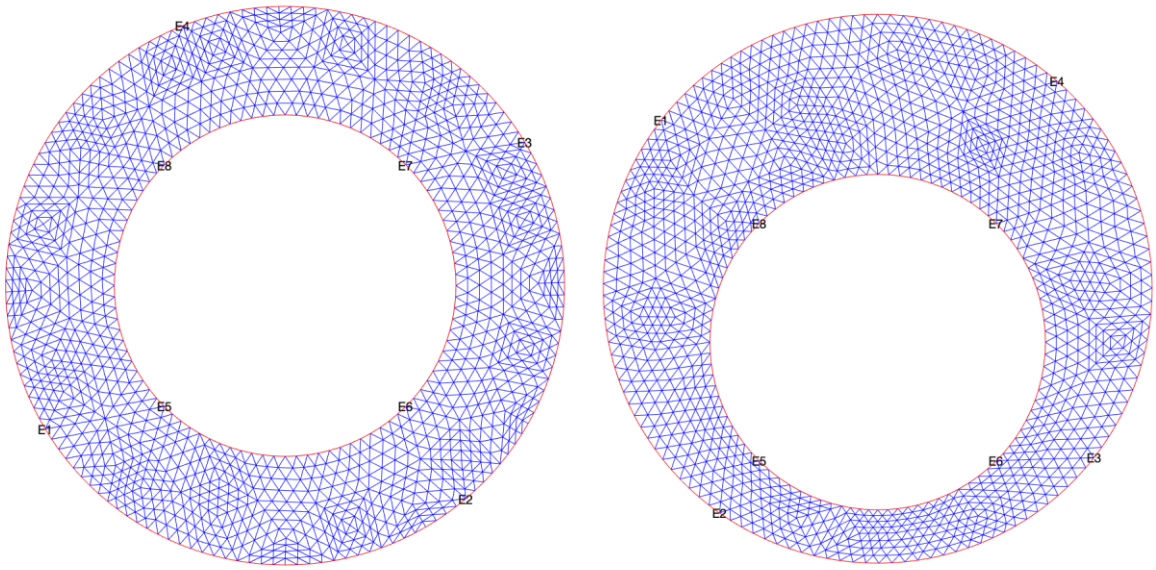


a b

Figure 3:Geometry and mesh used for numerical computations, a) concentric (e = 0) and b) eccentric (e = 0.5)

The geometric coordinates of the centroids, vertices, face centres and the face normal and tangent vectors of the control volumes in the mesh are obtained and stored prior to running the simulations to reduce computational cost. Appropriate boundary conditions are necessary in order to obtain accurate solutions of the governing equations in the annuli with or without inner pipe rotation. The axial and angular velocity at the outer wall follow the no-slip boundary condition hence the axial and tangential velocities of the vertex nodes that are in contact with the outer wall are set to zero. For the inner pipe wall, while the axial velocities of the vertex nodes are set to zero, in the simulations where the inner pipe is rotating the tangential velocities of the vertex nodes in contact with the inner pipe wall are set equal to $\omega_{max} r_1$. To perform the CFD simulations, the required axial pressure is first assumed, then the numerical equations are solved to generate the axial and tangential velocity fields that corresponds to the assumed axial pressure gradient. The computational procedure is given in Appendix D. The steady-state fluid flow iterative simulations were performed with the convergence criteria of 1e$^{-4}$. The rheological parameters of the simulated Newtonian and non-Newtonian fluids were obtained from literature (Bicalho et al., 2016; Diamante and Lan, 2014; Vieira Neto et al., 2014) and are given in Table 3.

Table 3: Rheological parameters of the simulated fluids

| **Fluid rheology type** | **K (Pa s$^n$)** | **n** | **$\tau_o$ (Pa)** |
|---|---|---|---|
| Newtonian | 0.0398 | 1 | 0 |
| Power law | 0.096 | 0.75 | 0 |
| Power law | 0.678 | 0.27 | 0 |
| Herschel-Bulkley | 0.6461 | 0.43 | 2.29 |

It should be noted that for the Newtonian fluid, $K = \mu$

## 5.0 Results and discussion

The combined effect of fluid rheology, fluid flowrate, eccentricity, and inner pipe rotation on the fluid dynamics and pressure loss for annuli flows was systematically analysed using the newly developed analytical and numerical models presented in this paper. Analytical calculations and numerical CFD simulations were performed, and the results obtained showed that unlike the Newtonian annuli fluid flows, the friction geometry parameter for non-Newtonian annuli flows is not only influenced by the eccentricity but also highly influenced by the inner pipe rotation speed, the fluid rheological parameters and input flowrate.

### 5.1 Validation of new analytical model

In order to validate the accuracy of the newly developed analytical model, a comparison of the friction geometry parameter calculated by the analytical model was performed using the model suggested by Caetano et al. (1992) for the friction geometry parameter for laminar flow of Newtonian fluids in annuli. Table 4 presents the values of the friction geometry parameter obtained for different pipe diameter ratios, using both methods for the flow of the Newtonian fluid in the concentric annuli. The values obtained using the new analytical model matched perfectly with that of Caetano et al. (1992) with an absolute error of ±0%. The Caetano et al. (1992) model is presented in Appendix A.

Table 4: Friction geometry parameter values at different pipe diameter ratios for the concentric annuli (e =0), obtained from Caetano et al. (1992) and the new analytical model for the flow of Newtonian fluids

| **Pipe diameter ratio** | **Friction geometry parameter (e = 0)** | |
|---|---|---|
| | **Caetano et al. (1992)** | **New analytical model** |
| 0.1 | 22.3430 | 22.3430 |
| 0.2 | 23.0881 | 23.0881 |
| 0.3 | 23.4612 | 23.4612 |
| 0.4 | 23.6783 | 23.6783 |
| 0.5 | 23.8125 | 23.8125 |
| 0.6 | 23.8970 | 23.8970 |
| 0.7 | 23.9495 | 23.9495 |
| 0.8 | 23.9801 | 23.9801 |
| 0.9 | 23.9956 | 23.9956 |

Another comparison of the values obtained using the new analytical model to that which is presented in literature was performed for the validation the flow of non-Newtonian fluids in the eccentric annuli, without inner pipe rotation. The annuli pressure gradient for the flow of non-Newtonian Power law fluid at different wellbore eccentricities, predicted by the analytical model was also compared (Figure *4*) to that which was predicted by applying the pressure gradient correction factor developed by Haciislamoglu and Langlinais (1990) through a non-linear regression analysis using numerical data was obtained from the solution of the non-Newtonian fluid flow equations defined in the bipolar coordinate system. The Haciislamoglu and Langlinais (1990) correction factor was chosen as a reference for the new analytical model validation due to its reliability and applicability in the prediction of the pressure gradient for the flow of Power law fluids in the eccentric annuli (Bicalho et al., 2016; Pilehvari and Serth, 2009; Rojas et al., 2017; Sayindla et al., 2017; Tang et al., 2016; Tong et al., 2020). Although some studies have applied this pressure gradient correction factor for Yield Power Law fluids, these authors have neglected that the correction factor is only valid for Power law fluids (Dokhani et al., 2020). Haciislamoglu and Langlinais (1990) reported that the accuracy of the pressure gradient correction factor was about ±5%. However, the comparison of the analytical model developed in this study showed a maximum deviation of about 7%. The Haciislamoglu and Langlinais (1990) pressure gradient correction factor equation is presented in Appendix B.

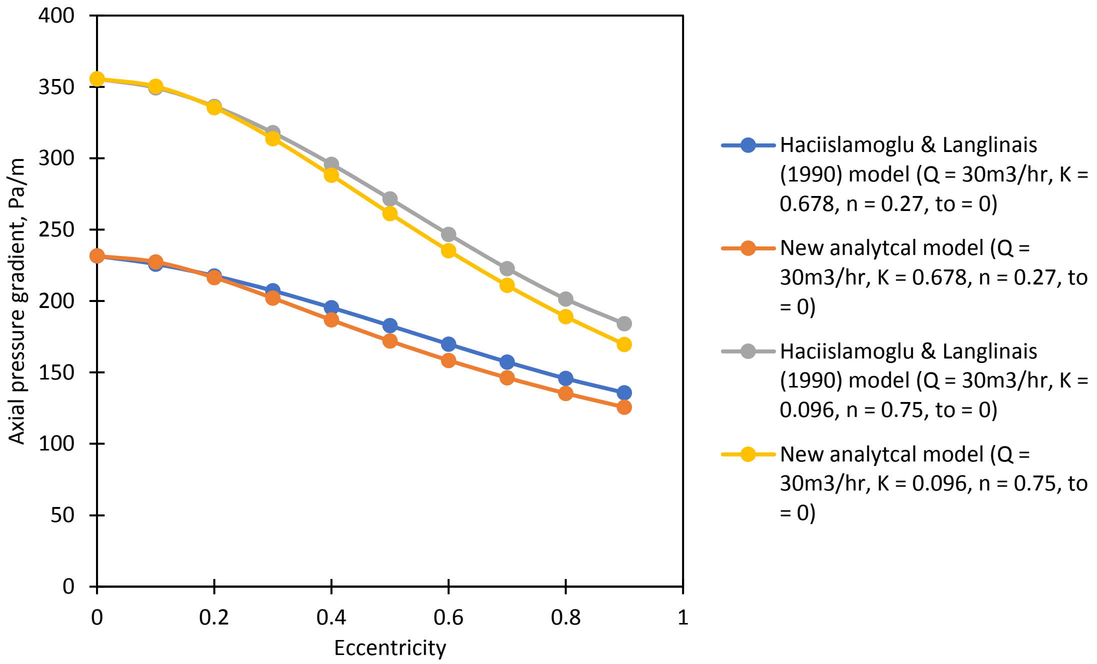


Figure 4: Comparison of the annuli frictional pressure gradient obtained from new analytical model vs that of Haciislamoglu and Langlinais (1990) for Power law annuli fluid flow

The favourable comparison of the analytical model for the friction geometry parameter and the consequent frictional pressure gradient for annuli flows provides proof that the model can be applied with confidence for the analysis and prediction of the flow dynamics for both Newtonian and non-Newtonian fluid flows in the concentric and eccentric annuli. However, the new models presented in this study provides an additional benefit of considering the combined effect of fluid rheology, flowrate, eccentricity, and inner pipe rotation while analysing Newtonian and non-Newtonian annuli fluid flows and performing the pressure loss calculations.

### 5.2 Influence of eccentricity

The distribution of the velocity fields for the flow of Newtonian and non-Newtonian fluids in the concentric annuli is generally uniform across the circumference of the annuli. However, when the flowrate is held constant, an increase in the eccentricity leads to an asymmetric distribution of the flow field, where higher fluid velocities exist in the larger flow areas of the annuli, in contrast to lower fluid velocities in the smaller or reduced flow areas. The severity of the induced asymmetry in the velocity fields is dependent on the level of inner pipe eccentricity. It was observed that the distribution of the velocity field, the position and value of the maximum velocity in the annuli is highly dependent on the flow regime and the rheological properties of the fluid.
Figure *5* to Figure 8 presents the visualisation of the axial velocity fields obtained from CFD simulations using the numerical model. These simulations were performed to analyse the behaviour of the flow for all the fluid types (**Error! Reference source not found.**) at a constant flowrate of 30 $m^3$/hr without inner pipe rotation.
Figure *5* to Figure 8 shows the axial velocity fields obtained for both Power law fluids simulated in this study. Even though the shear stress to shear rate relationship for both fluids are governed by the Power law rheological model, at the same fluid flowrate, the velocity field distribution in the concentric and eccentric annulus were dependent on the rheological parameters of the fluids. At a constant fluid flowrate, an increase in eccentricity produced a corresponding decrease in the axial frictional pressure gradient for both the Newtonian and non-Newtonian fluids. This is mainly because a larger portion of the fluids flow though the larger regions of the eccentric annuli where a lesser flow resistance is experienced. The reduction in pressure loss due to the increase in the eccentricity has also been reported by several works in literature (Dokhani et al., 2020; Silva and Shah, 2000).

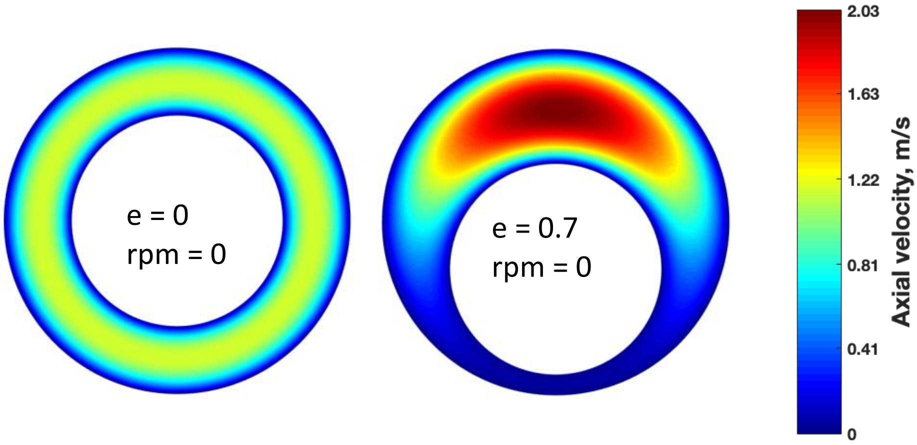


Figure 5: Axial velocity fields obtained for the Power law fluid (K = 0.096, n = 0.75, $\tau_o$ = 0) flowing at 30 $m^3$/hr in the concentric (e = 0) and eccentric (e = 0.7) annuli

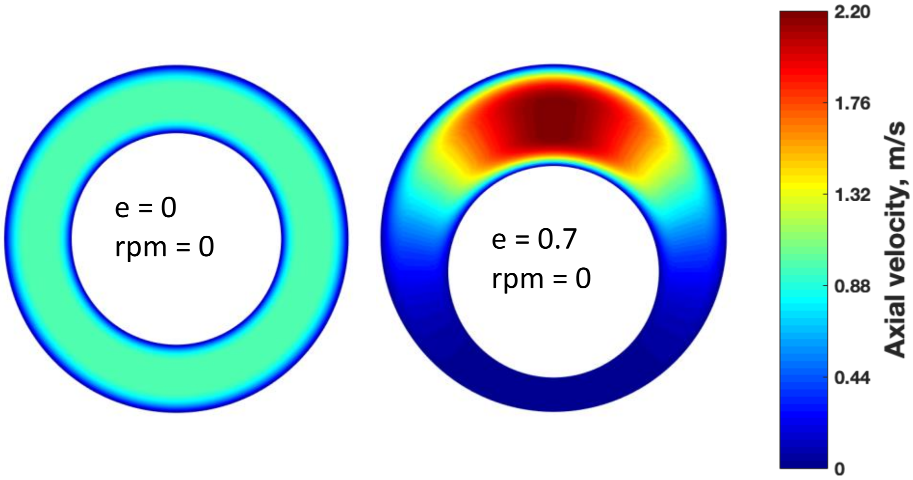


Figure 6: Axial velocity fields obtained for the Herschel-Bulkley fluid (K = 0.6461, n = 0.43, $\tau_o$ = 2.29) flowing at 30 $m^3$/hr in the concentric (e = 0) and eccentric (e = 0.7) annuli

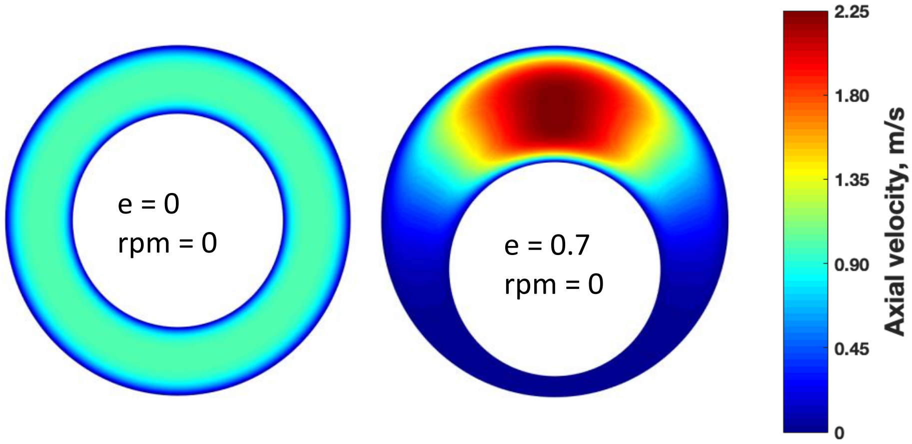


Figure 7: Axial velocity fields obtained for the Power law fluid (K = 0.678, n = 0.27, $\tau_o$ = 0) flowing at 30 $m^3$/hr in the concentric (e = 0) and eccentric (e = 0.7) annuli

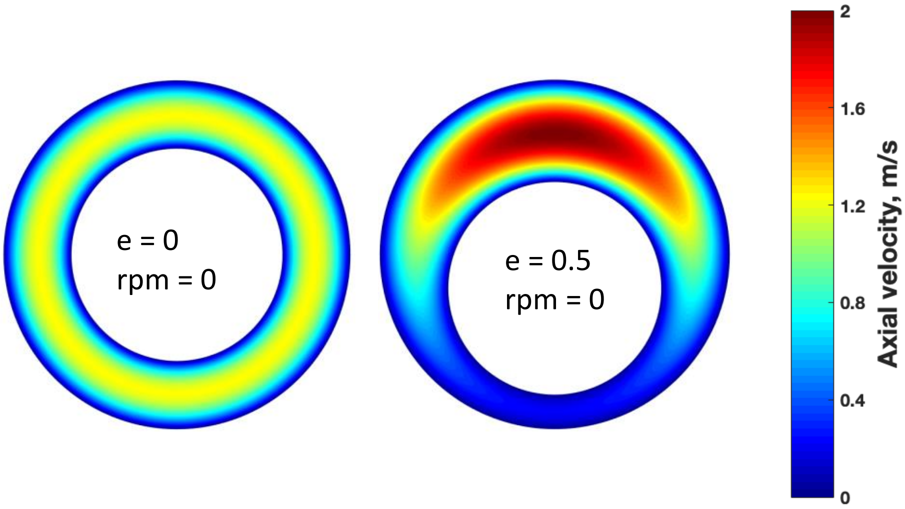


Figure 8: Axial velocity fields obtained for the Newtonian fluid (K = 0.0398, n = 1, $\tau_o$ = 0) flowing at 30 $m^3$/hr in the concentric (e = 0) and eccentric (e = 0.7) annuli

However, the degree to which the eccentricity influences the axial frictional pressure gradient is dependent on the fluid rheology. Unlike the case of the Newtonian fluid flow, the friction geometry parameter for the non-Newtonian fluid flow is not only influenced by the inner pipe eccentricity but also influenced by the rheological parameters of the fluids. The friction geometry parameter for the different fluids obtained from the analytical model is presented in Figure 9.

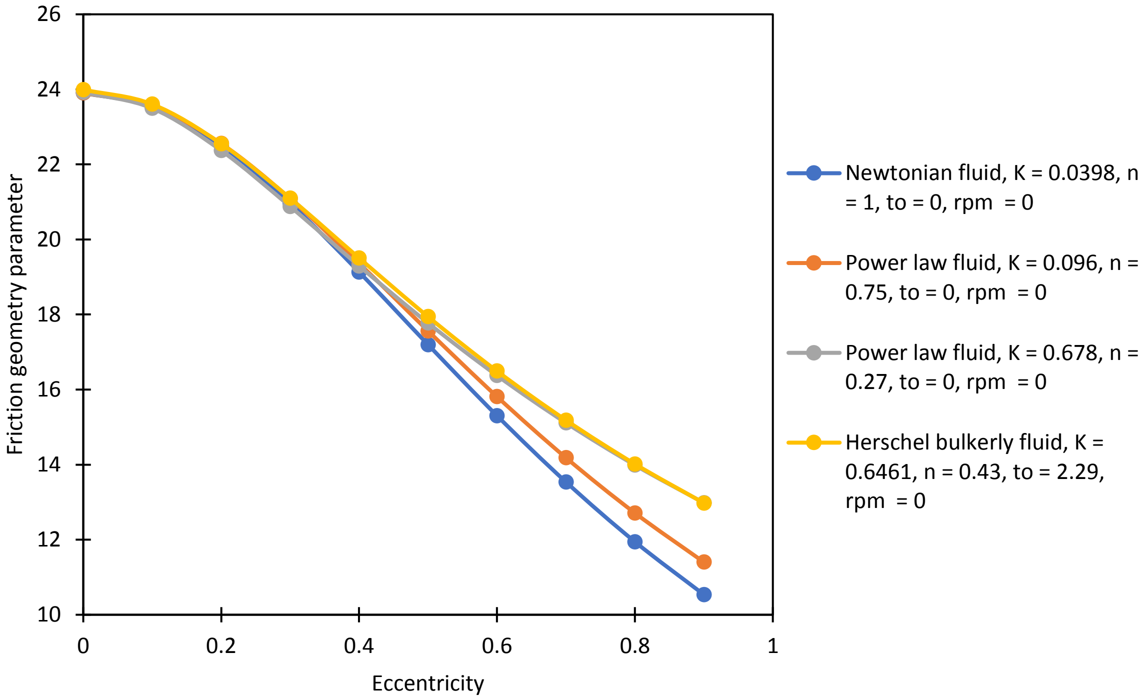


Figure 9: Influence of eccentricity and fluid rheology on the annuli friction geometry parameter for the different simulated fluids

It can be deduced that while the friction geometry parameter values for all the simulated fluids in the concentric annuli or at low eccentricities are approximately the same, at higher inner pipe eccentricities, the fiction geometry parameter for the non-Newtonian fluids significantly deviates from that of the Newtonian fluid to an extent that is dependent on the fluid properties. The results obtained from the analytical and numerical model ascertains that at a given eccentricity, the friction geometry parameter for the Newtonian fluid is constant. However, for the non-Newtonian fluids, the effect of the eccentricity on the friction geometry parameter, the annuli friction factor, and the corresponding axial frictional pressure gradient is dependent on the fluid rheological parameters. Figure 10 to Figure 12 present the comparison of the axial frictional pressure gradient obtained from the new analytical and numerical models for the flow of the different fluid rheology types at different fluid flowrates in the concentric and eccentric annuli.

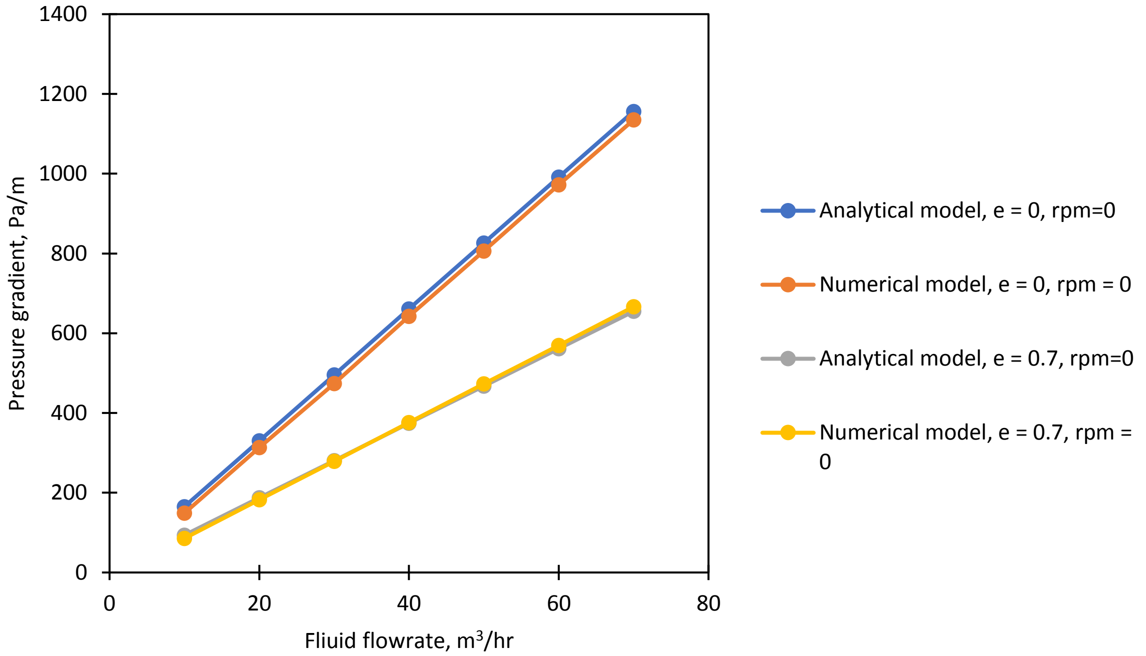


Figure 10: Comparison of the frictional pressure gradient obtained from the numerical and analytical model for the flow of the Newtonian fluid (K = 0.0398, n = 1, $\tau_o$ = 0) at different flowrates in the concentric (e = 0) and eccentric (e = 0.7) annuli

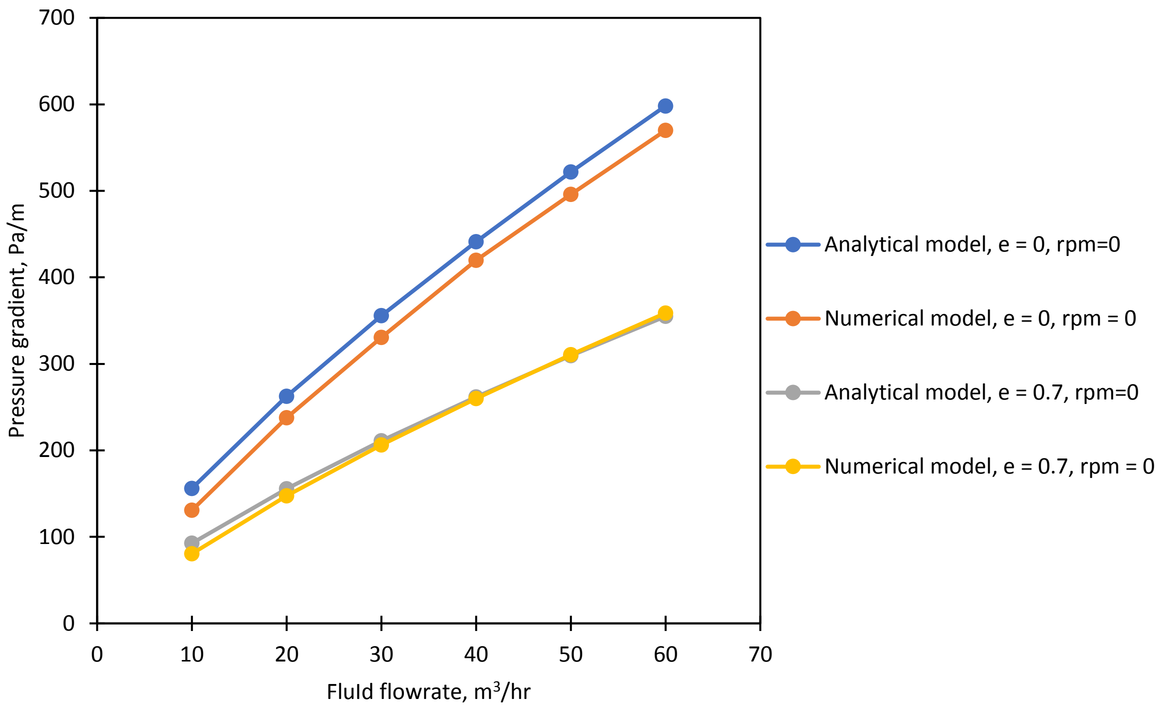


Figure 11: Comparison of the frictional pressure gradient obtained from the numerical and analytical model for the flow of the Power law fluid (K = 0.096, n = 0.75, $\tau_o$ = 0) at different flowrates in the concentric (e = 0) and eccentric (e = 0.7) annuli.

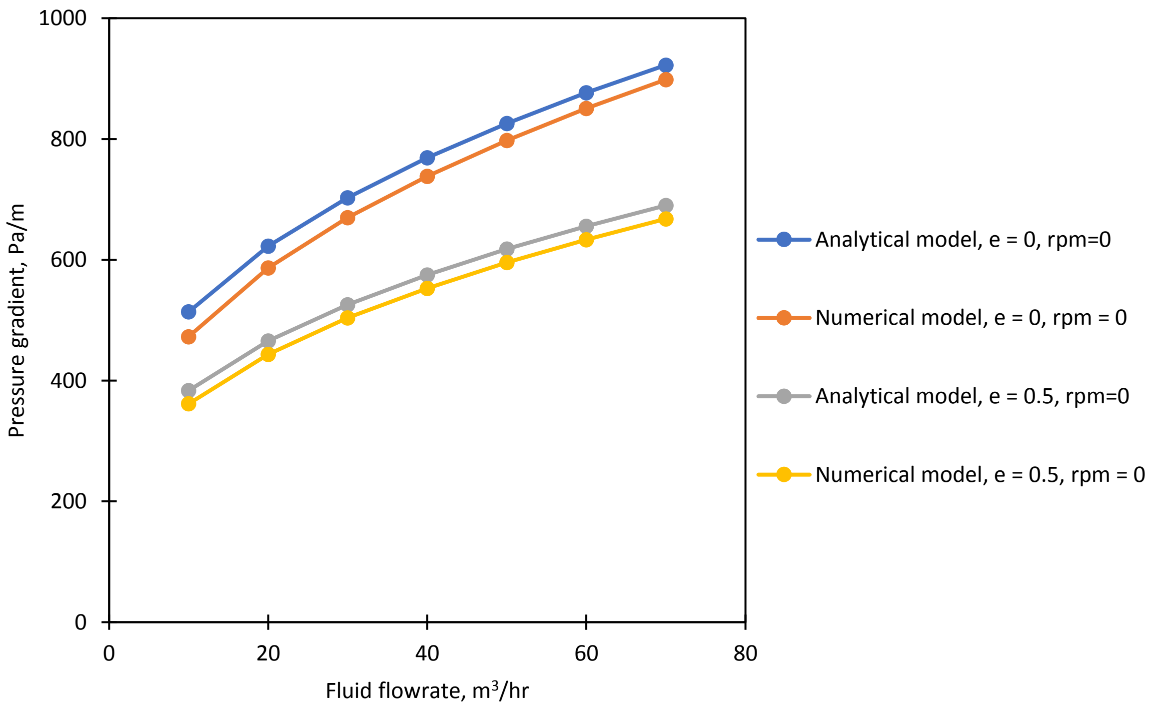


Figure 12: Comparison of the frictional pressure gradient obtained from the numerical and analytical model for the flow of the Herschel-Bulkley fluid (K = 0.6461, n = 0.43, $\tau_o$ = 2.29) at different flowrates in the concentric (e = 0) and eccentric (e = 0.5) annuli

The analytical model and numerical CFD simulations predicted a decrease in the axial frictional pressure gradient with an increase in eccentricity without inner pipe rotation and the comparison showed very good agreement with a maximum error of about 10%.

### 5.3 Influence of inner pipe rotation

The combined effect of eccentricity and inner pipe rotation has a strong influence on the friction geometry parameter of the flow and thereby influences the friction factor or frictional pressure gradient for non-Newtonian helical fluid flow through the annuli. However, there is no significant impact of the inner pipe rotation on the friction geometry parameter for Newtonian fluid flow in the concentric and eccentric annuli, even though the increase in the eccentricity still produces a corresponding decrease in the frictional pressure gradient. The friction geometry parameter developed for the Newtonian fluids cannot be applied to perform accurate predictions of the frictional pressure losses for flow of non-Newtonian fluids in the annuli with or without inner pipe rotation. The results obtained from the analytical and numerical model simulations show that the impact of the inner pipe rotation on the fluid velocity distribution and frictional pressure losses for non-Newtonian fluids is highly dependent on the rheological properties of the fluid, fluid flowrate, eccentricity, and the pipe diameter ratio of the annuli. The introduction of inner pipe rotation generates a tangential fluid velocity component that varies in the radial and angular direction (eccentric cases) in the annuli space and in a manner that is dependent on the eccentricity and rheological parameters of the fluids. The tangential velocity field has its maximum value at the inner pipe wall, decreases in the radial direction and is zero at the outer pipe wall due to the no-slip effect (
Figure *13* and
Figure *14*).

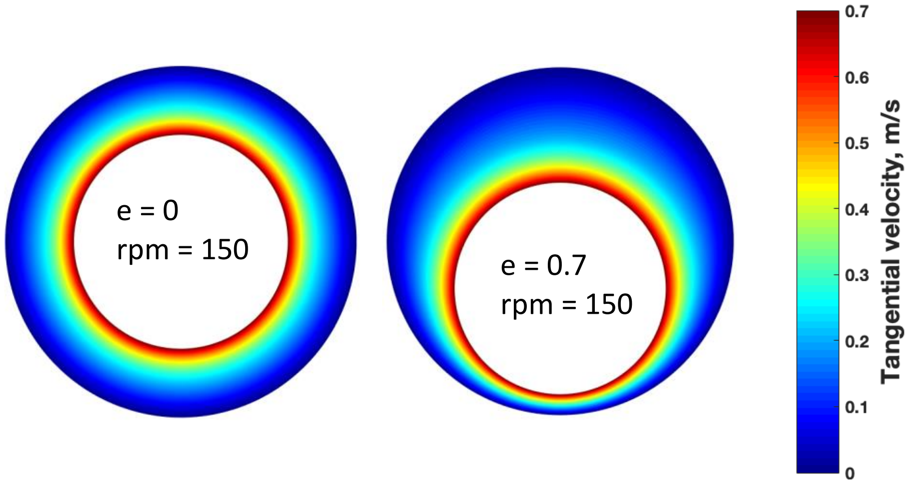


Figure 13: Tangential velocity distribution for the flow of the Power law fluid (K = 0.096, n = 0.75, $\tau_o$ = 0) at a flowrate of 30 $m^3$/hr and an inner pipe rotary speed of 150 rpm in the concentric (e = 0) and eccentric (e = 0.7) annuli

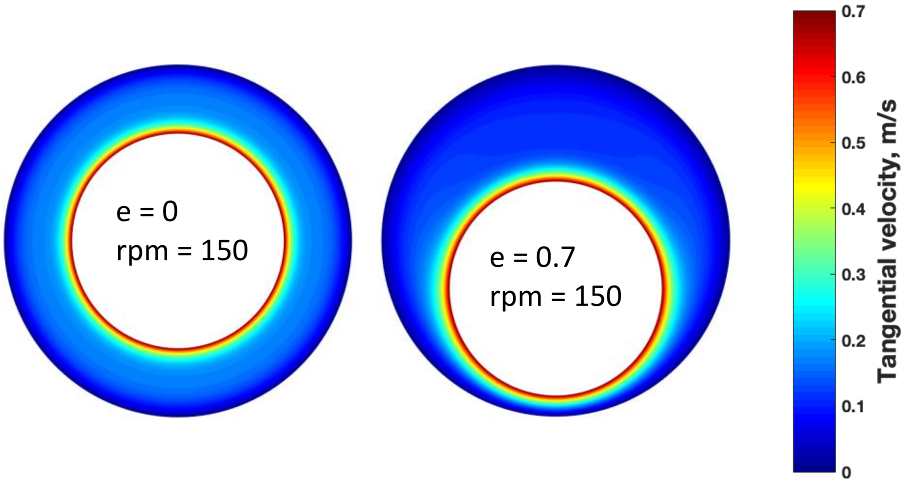


Figure 14: Tangential velocity distribution for the flow of the Power law fluid (K = 0.678, n = 0.27, $\tau_o$ = 0) at a flowrate of 30 $m^3$/hr and an inner pipe rotary speed of 150 rpm in the concentric (e = 0) and eccentric (e = 0.7) annuli

From Figure *13* and Figure *14*, it is observed that although both of the fluids are characterised by the Power law rheological model and flowing at the same flowrate and inner pipe rotation, the shape and size of the velocity profiles were a function of the rheological parameters of the fluid. Figure 15 to Figure 18 are plots that show the actual values and shape of the tangential velocity profile in the largest and smallest radial gap in the eccentric (e = 0.7) annuli for pipe rotation speeds in the range of 120 to 300 rpm. While the tangential velocities of the two fluids differ significantly in the largest radial gap, the tangential velocities in the smallest radial gap in the annuli approached the same value at the different rotary speeds. For the flow of non-Newtonian shear-thinning fluids through the annuli, the introduction of the inner pipe rotation changes the fluid viscosity at every local position in the annuli. This change in the fluid local viscosity in the annuli space is a function of the magnitude of the axial and tangential shear rate and is highly influenced by pipe eccentricity and fluid rheology.

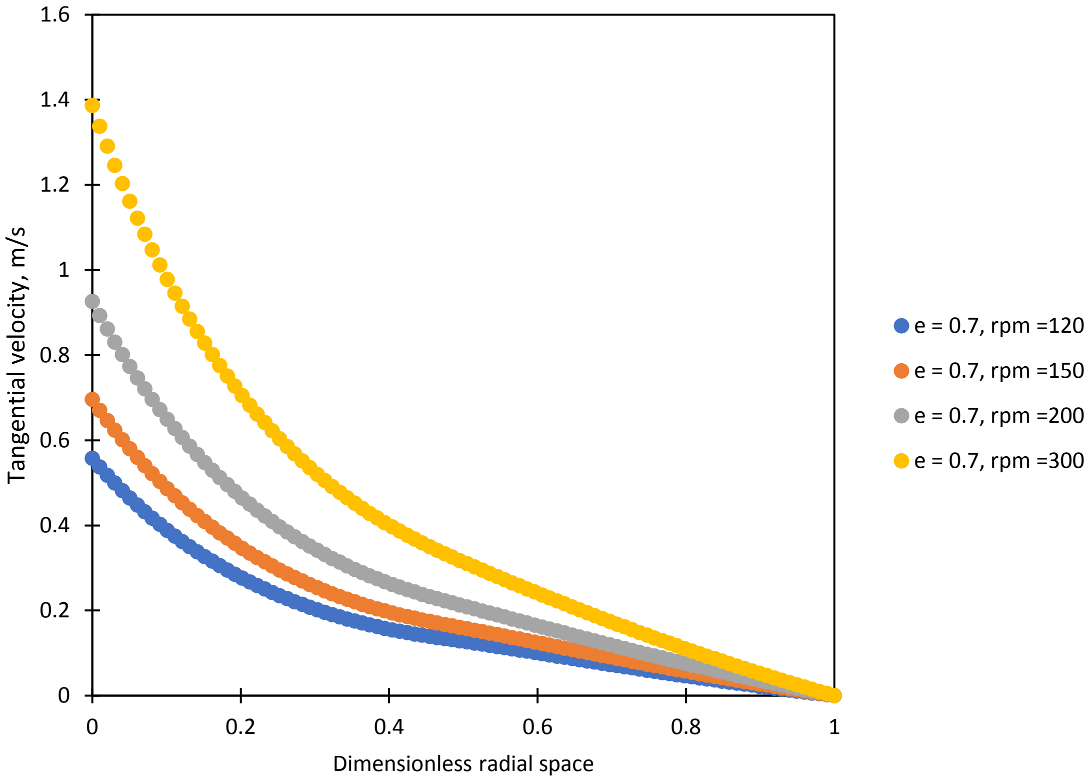


Figure 15: Tangential velocity profiles of the Power law fluid (K = 0.096, n = 0.75, $\tau_o$ = 0) in the largest radial gap of the eccentric (e = 0.7) annuli at different inner pipe rotation speeds

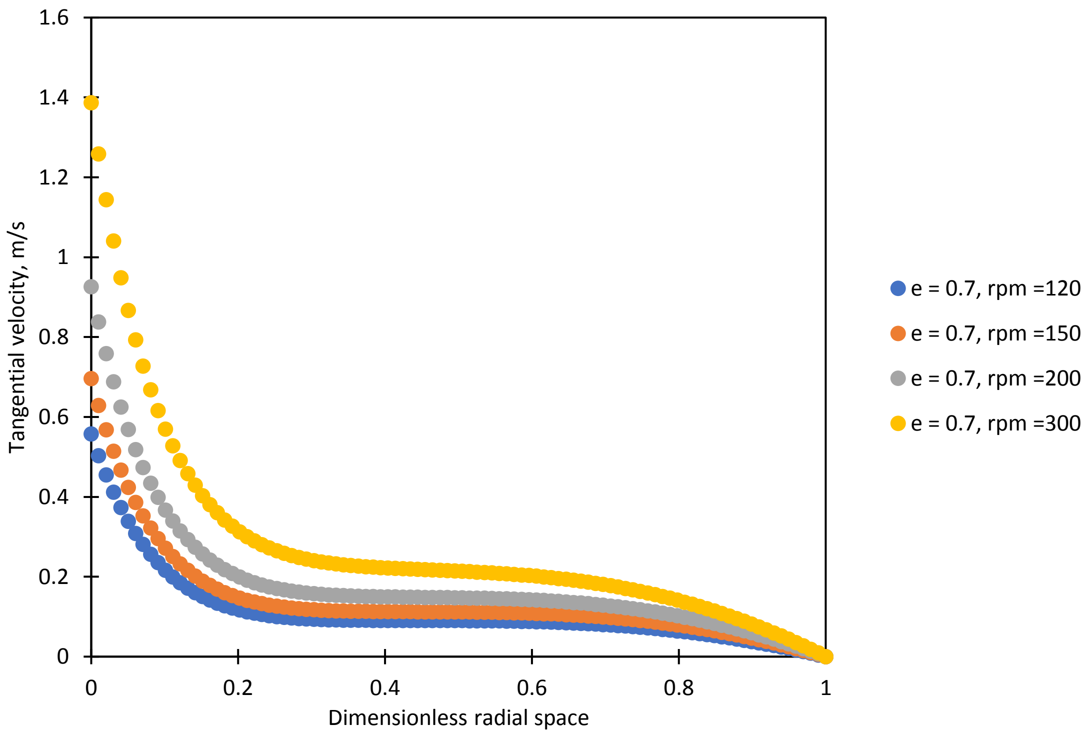


Figure 16: Tangential velocity profiles of the Power law fluid (K = 0.678, n = 0.27, $\tau_o$ = 0) in the largest radial gap of the eccentric (e = 0.7) annuli at different inner pipe rotation speeds

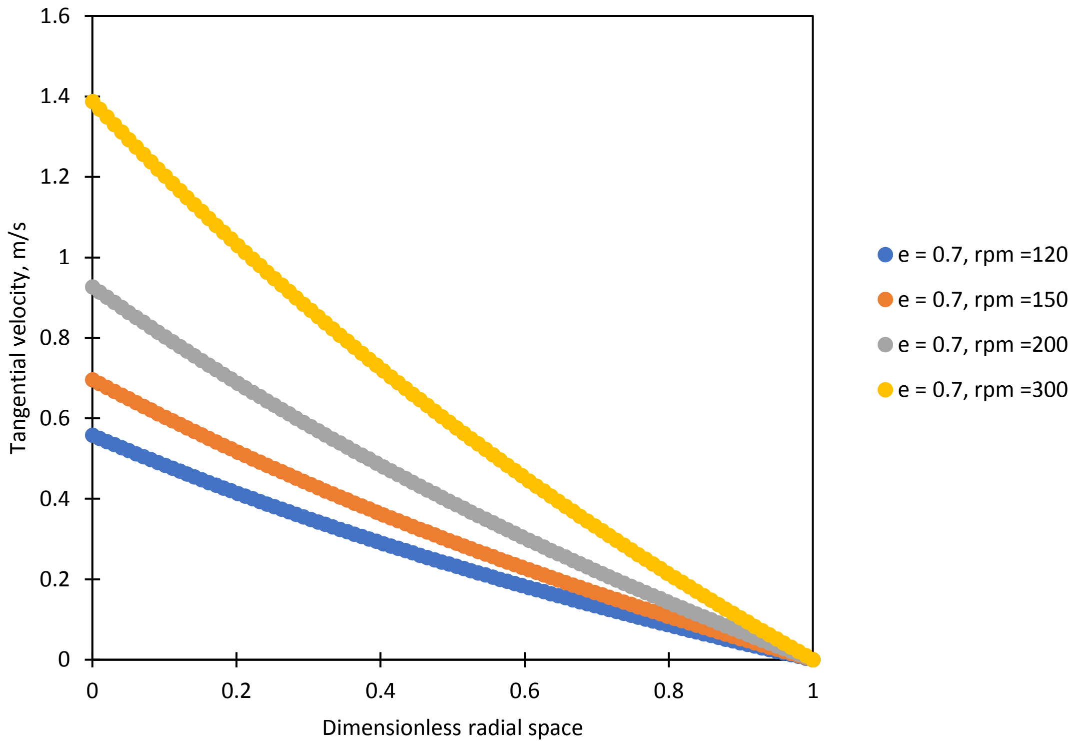


Figure 17: Tangential velocity profiles of the Power law fluid (K = 0.096, n = 0.75, $\tau_o$ = 0) in the smallest radial gap of the eccentric (e = 0.7) annuli at different inner pipe rotation speeds

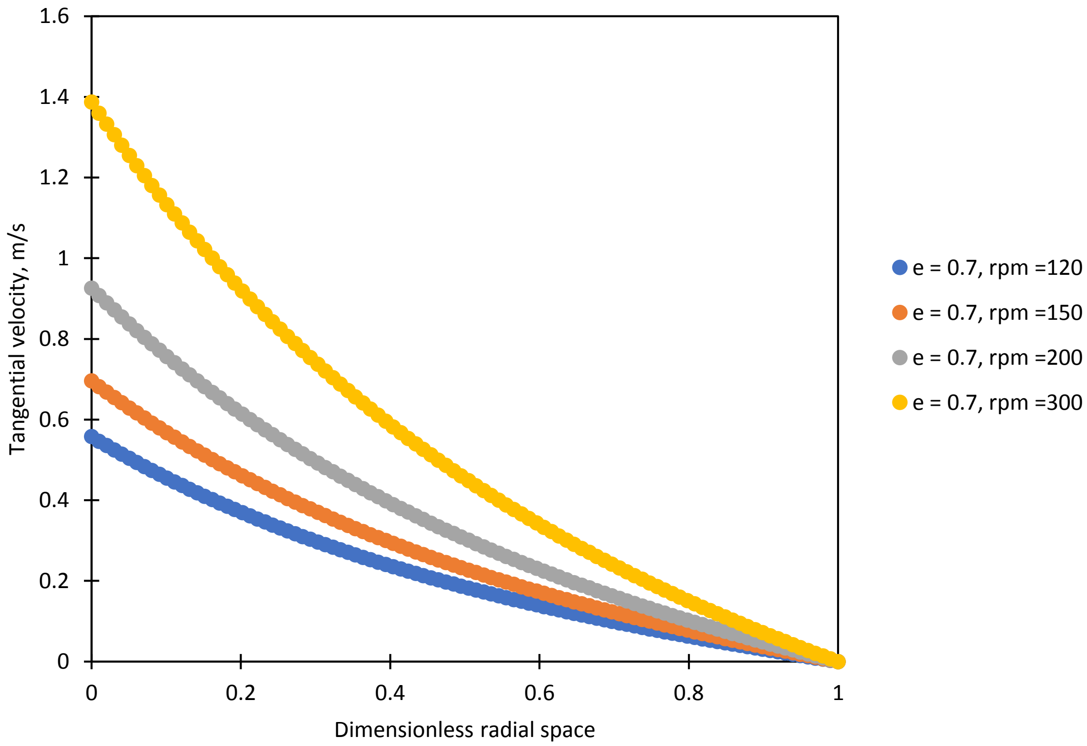


Figure 18: Tangential velocity profiles of the Power law fluid (K = 0.678, n = 0.27, $\tau_o$ = 0) in the smallest radial gap of the eccentric (e = 0.7) annuli at different inner pipe rotation speeds

Figure 19 and Figure 20 present the viscosity profile of the Power law fluid in the concentric and eccentric annulus at different inner pipe rotation speeds and at a constant fluid flowrate of 30 $m^3$/hr. It can be observed that at the same flow conditions, higher viscosity values are seen in the larger radial gap of the eccentric annuli when compared to fields in the concentric annuli, due to the reduction of the flow resistance in those regions. However, lower fluid viscosity values exist in the smallest radial gap in the annuli and an increase in the inner pipe rotary speed produced a decrease in the fluid viscosity for the shear-thinning non-Newtonian fluids.

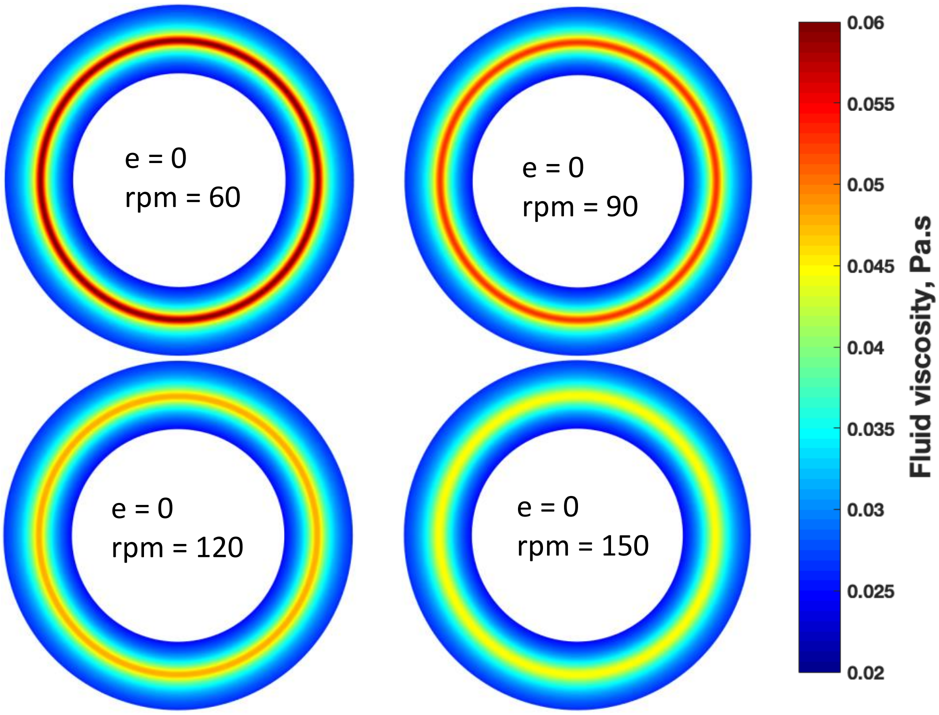


Figure 19: Reduction of the Power law fluid (K = 0.096, n = 0.75, $\tau_o$ = 0) viscosity in the concentric (e = 0) annulus with an increase in the inner pipe rotary speed

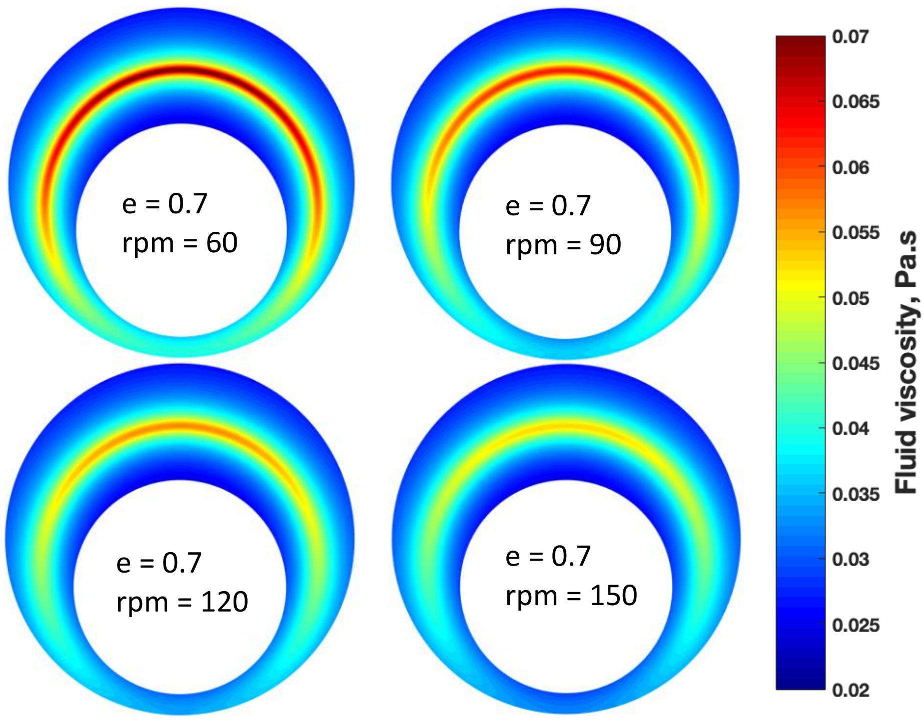


Figure 20: Reduction of the Power law fluid (K = 0.096, n = 0.75, $\tau_o$ = 0) viscosity in the eccentric (e = 0.7) annulus with increase in the inner pipe rotary speed

The viscosity field in the smallest radial gap in the annuli decreased with inner pipe rotation significantly more when compared to the other areas in the annuli due to its smaller radial distance and relatively higher tangential velocities. The inner pipe rotation produced no significant effect on the distribution of the velocity fields for the Newtonian and non-Newtonian fluids in the concentric annuli. However, in the eccentric annuli, while the inner pipe rotation had no significant influence on the velocity fields for the Newtonian flow, for the non-Newtonian fluids, the inner pipe rotation redistributed the velocity fields in the eccentric annuli and improved the flow in the regions with the smaller radial gap in the annuli.
To visualise the effect of the inner pipe rotation on the velocity fields, the fluid axial velocity profiles at the largest and smallest radial gap in the annuli is given in Figure 21 to Figure 24 for the different Power law fluids at a flowrate of 30 $m^3$/hr. An increase in the inner pipe rotation leads to an increase in the fluid velocity in the smallest region of the annuli for the non-Newtonian fluids. However, if the fluid flowrate is constant, the fluid velocity in the larger areas are as a result, reduced. Comparing Figure 21 to Figure 22 and Figure 23 to Figure 24, it can be seen that the Power law fluid with the lower flow behaviour index had a higher decrease in the axial velocity in the largest radial gap as well as a higher increase in the axial velocity in the smallest radial gap in the annuli. Thus, it is evident that the effect of the inner pipe rotation on the axial velocity fields is significantly influenced by the fluid rheology and eccentricity.

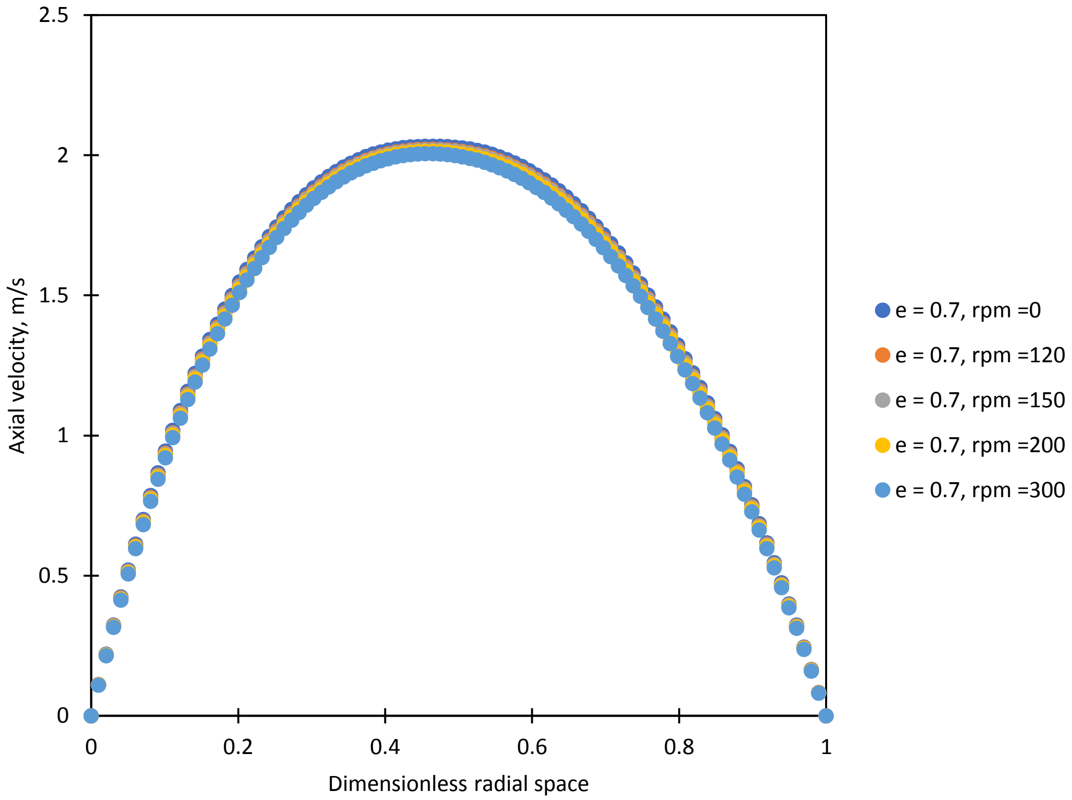


Figure 21: Reduction of the axial velocity of the Power law fluid (K = 0.096, n = 0.75, $\tau_o$ = 0) in the largest radial gap of the eccentric (e = 0.7) annulus with an increase in the inner pipe rotation speed

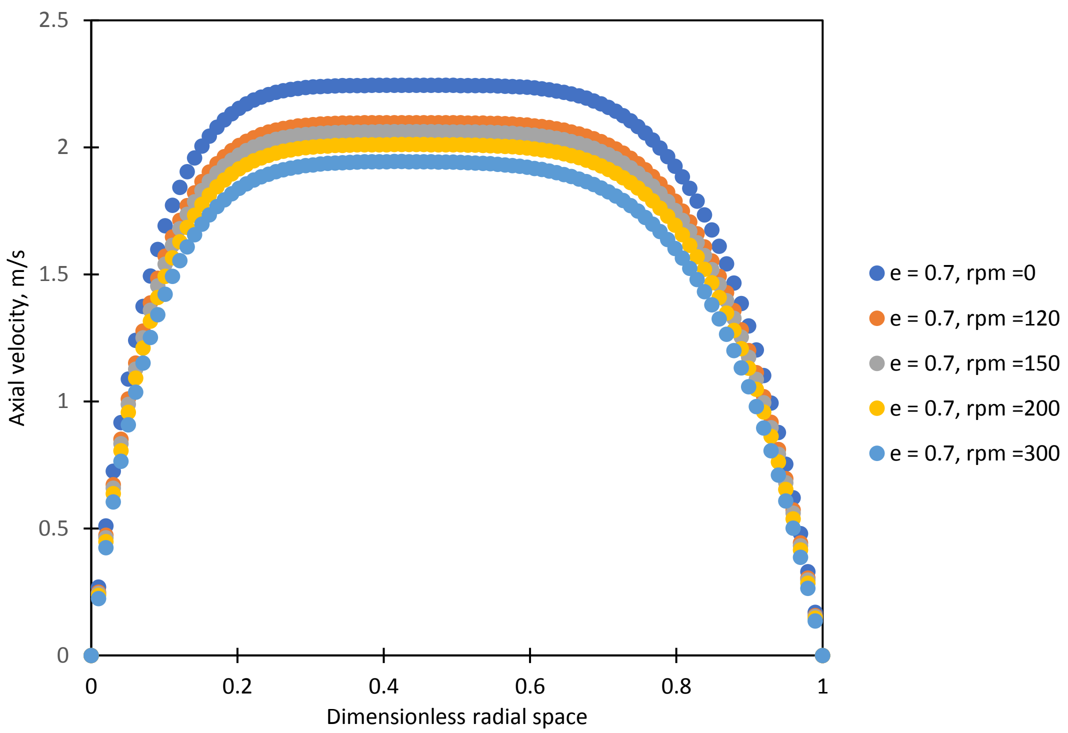


Figure 22: Reduction of the axial velocity of the Power law fluid (K = 0.678, n = 0.27, $\tau_o$ = 0) in the largest radial gap of the eccentric (e = 0.7) annulus with an increase in the inner pipe rotation speed

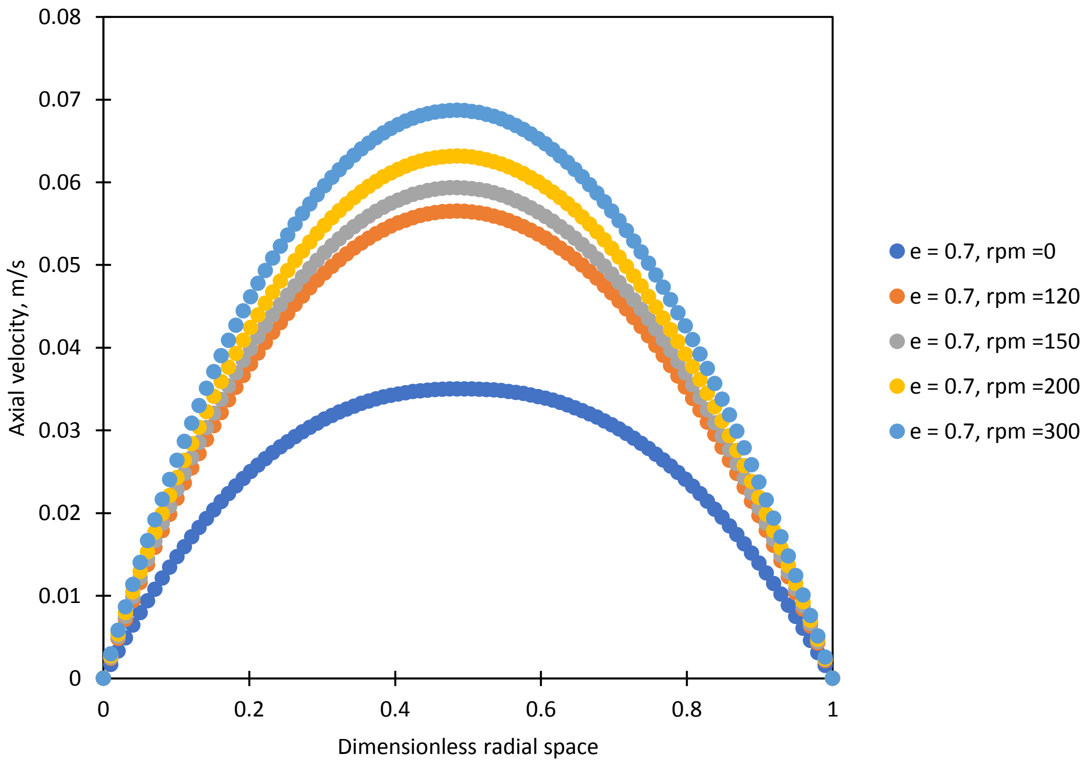


Figure 23: Improvement of the axial velocity of the Power law fluid (K = 0.096, n = 0.75, $\tau_o$ = 0) in the smallest radial gap of the eccentric (e = 0.7) annulus with an increase in the inner pipe rotation speed

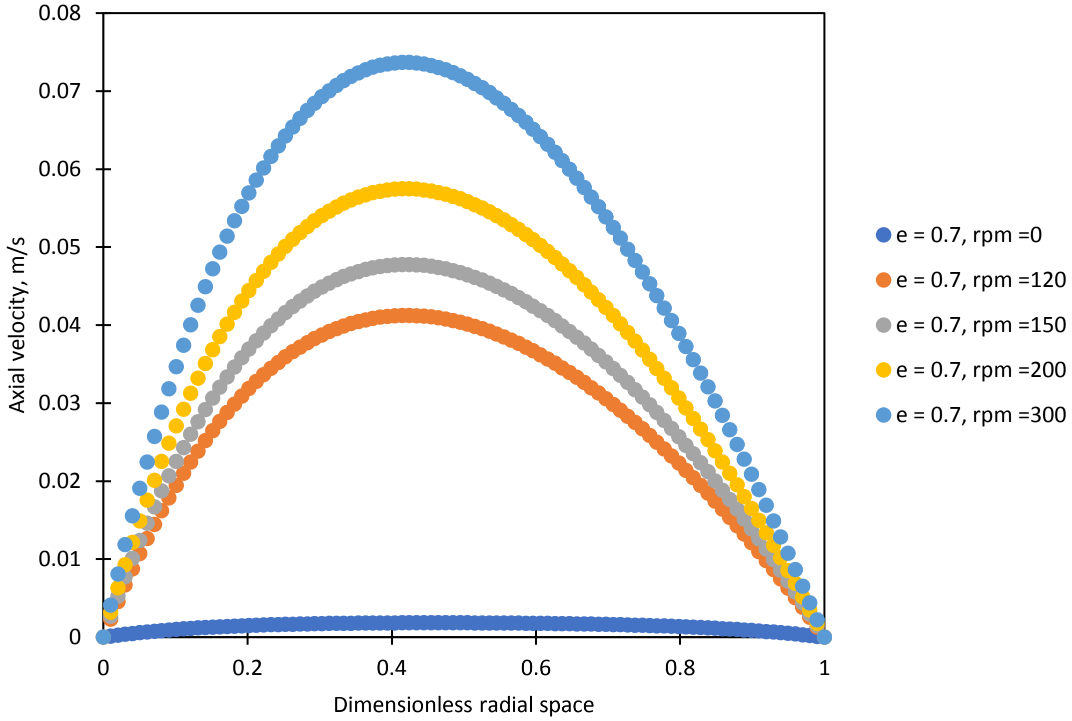


Figure 24: Improvement of the axial velocity of the Power law fluid (K = 0.678, n = 0.27, $\tau_o$ = 0) in the smallest radial gap of the eccentric (e = 0.7) annulus with increase in the inner pipe rotation speed

Inner pipe rotation has a significant influence on the fluid dynamics in the annuli. It was observed that changes in the inner pipe rotation speed also produces a significant influence on the annuli friction geometry parameter. While inner pipe rotation has no significant influence on the friction geometry parameter for the Newtonian fluids, the effect of the inner pipe rotation on the friction geometry parameter for the different non-Newtonian fluids are shown in Figure 25 to Figure 28.

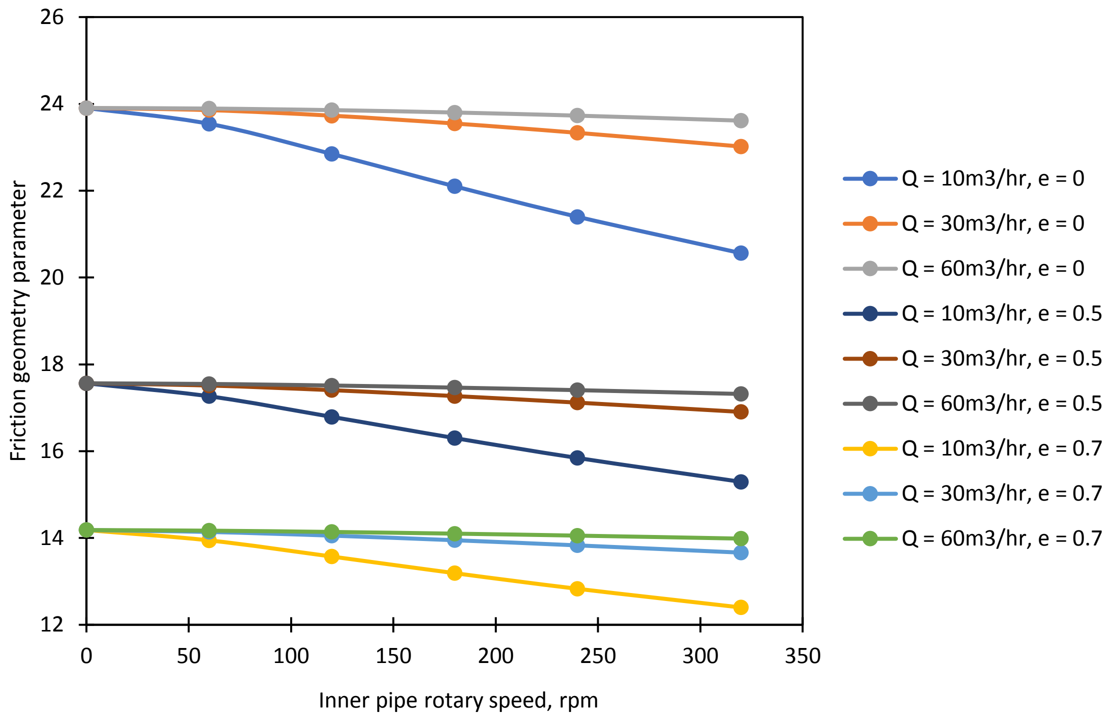


Figure 25: Changes in the annuli frictional geometry parameter for the Power law fluid (K = 0.096, n = 0.75, $\tau_o$ = 0) due to an increase in inner pipe rotary speed at different fluid flowrates

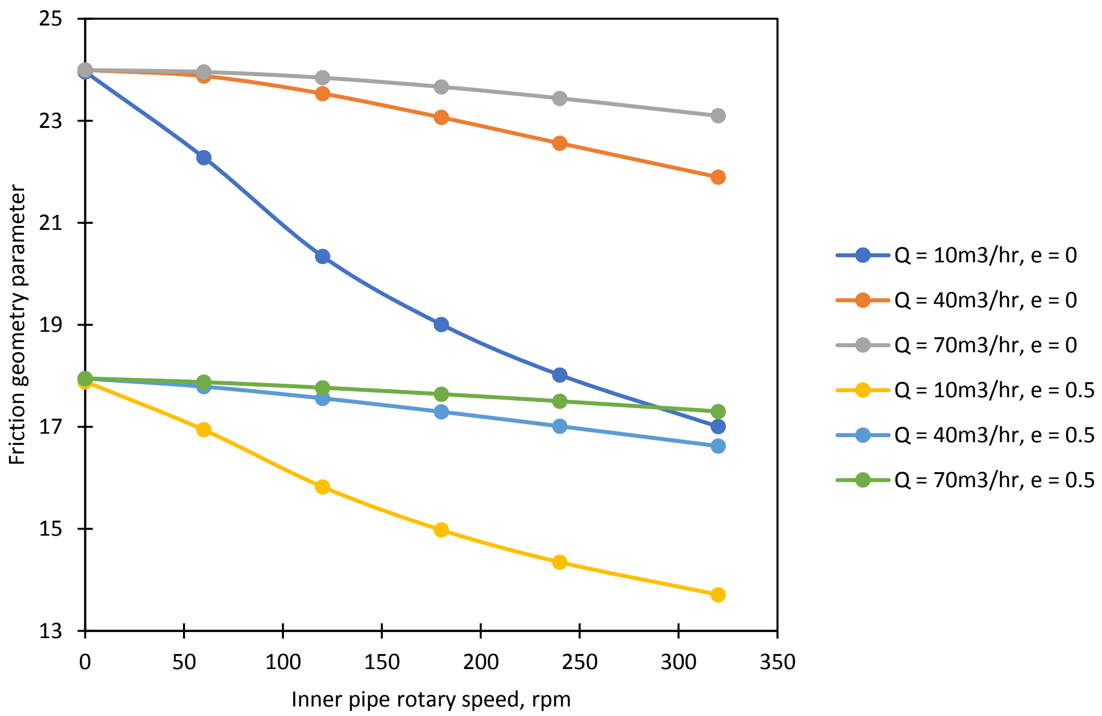


Figure 26: Changes in the annuli frictional geometry parameter for the Herschel-Bulkley fluid (K = 0.6461, n = 0.43, $\tau_o$ = 2.29) due to an increase in inner pipe rotary speed at different fluid flowrates

An increase in the inner pipe rotation speed led to a decrease in the friction geometry parameter for all the non-Newtonian fluids and it was observed that the effect of the inner pipe rotation on the friction geometry parameter was not only dependent on the fluid rheology and eccentricity but also significantly dependent on the fluid flowrate. Figure 25 and Figure 26 show that as the fluid flowrate was increased, the influence of the pipe rotation on the friction geometry parameter significantly decreased. This is one of the fundamental reasons why the effect of the inner pipe rotation on the flow behaviour of the fluids flowing under the turbulent flow regime is somewhat insignificant. There have also been several studies that have reported the negligible effect of the inner pipe rotation at high fluid circulation rates or turbulent flow conditions (Erge et al., 2014a, 2014b; Salubi et al., 2022).

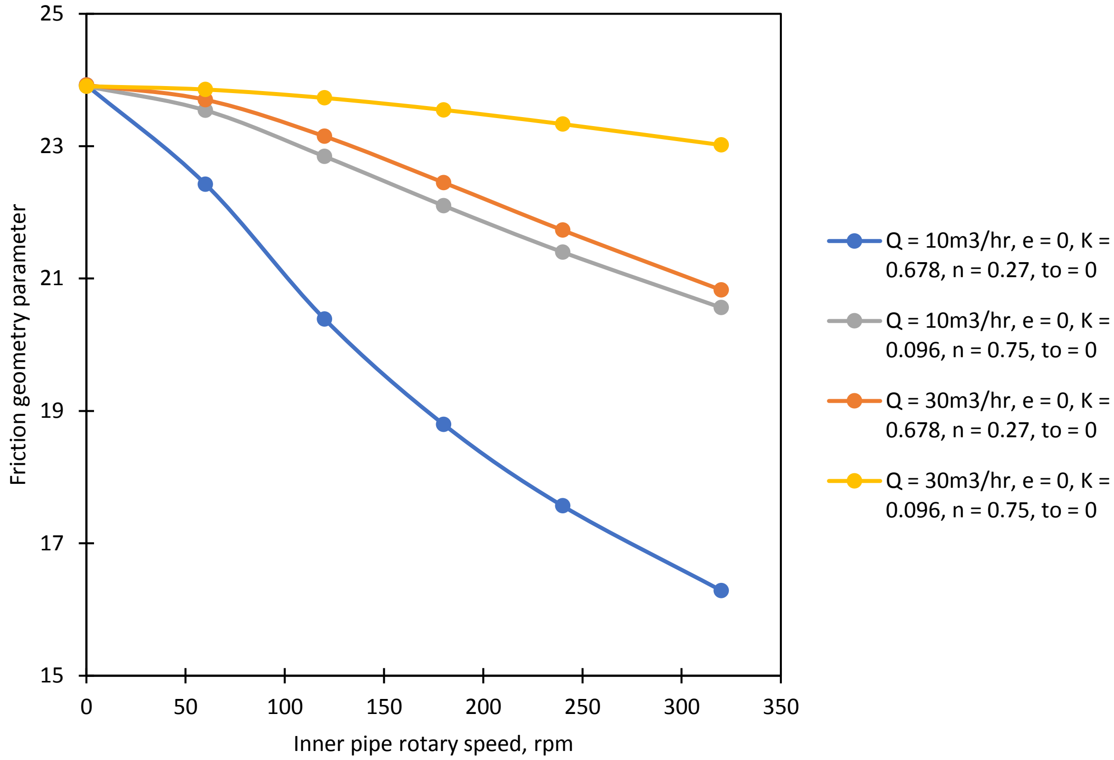


Figure 27: Effect of fluid rheology on the annuli frictional geometry parameter for the different Power law fluids in the concentric (e = 0) annuli due to an increase in inner pipe rotary speed at different fluid flowrates

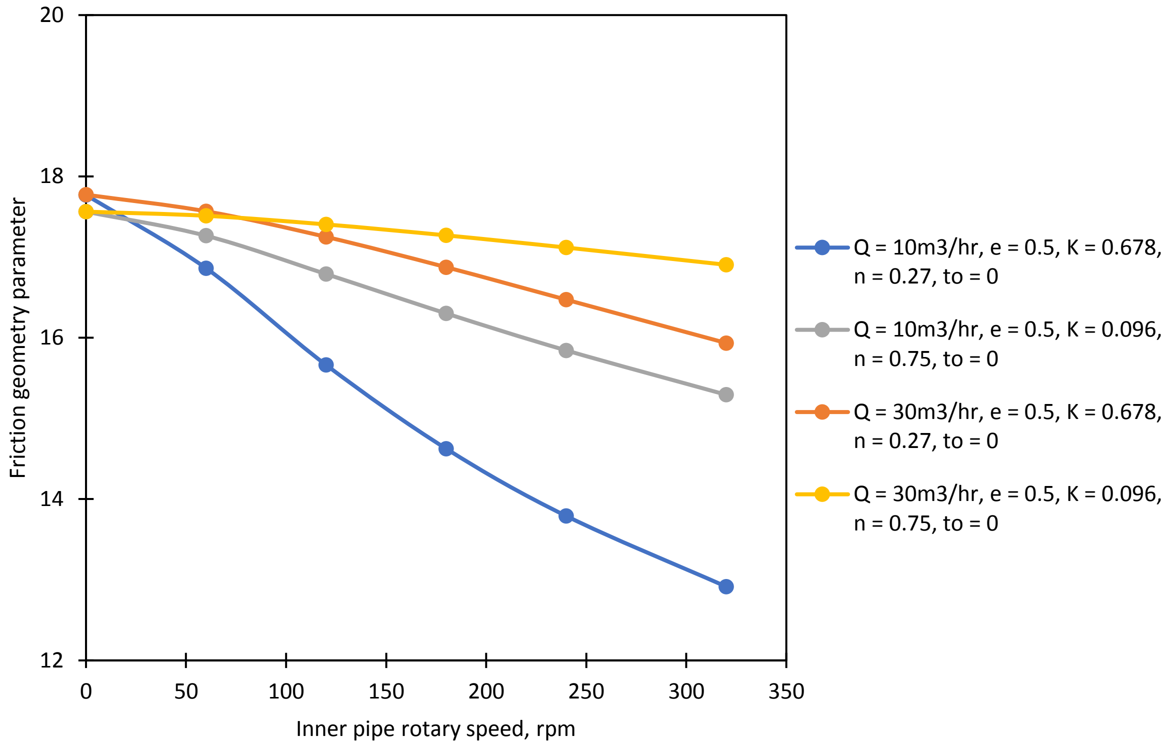


Figure 28: Effect of fluid rheology on the annuli frictional geometry parameter for the different Power law fluids in the concentric (e = 0) annuli due to an increase in inner pipe rotary speed at different fluid flowrates

For non-Newtonian fluids, the flowrate effect on the the friction geometry parameter due to pipe rotation is highly dependent on the eccentricity and fluid rheology of the fluids and if the rheological parameters are changed, the friction geometry parameter would differ even if the fluid rheology model or characteristics remains the same. However, for the Newtonian fluid the friction geometry parameter remains constant irrespective of the fluid viscosity. For example it can be deduced from Figure 25 to Figure 28 that the friction geometry parameter for the two Power law fluids differed significantly at various inner pipe rotation speeds, eccentricities, and fluid flowrates even though both fluids were characterised by the Power law rheological model.

**5.4 Influence of the annuli pipe diameter ratio**

The annuli pipe diameter ratio, $K_a = d_1/d_2$ is an important parameter that can also influence the friction geometry parameter along with the fluid rheology, eccentricity, flowrate, and inner pipe rotation. The effect of the inner pipe rotation on the friction geometry parameter in the lowest and highest annuli pipe diameter ratio is somewhat low when compared to the other pipe diameter ratios. This is because at low pipe diameter ratios, the size of the inner pipe is too small when compared to the outer pipe and thus the inner pipe rotation cannot generate enough tangential force to compete with the axial force of the flow. At very high pipe diameter ratios, the space between the inner and outer pipe is small and thus generates a high axial shear force that largely exploits the shear thinning properties of the fluid. Thus, the axial force dominates as the inner pipe rotation in this case, cannot thin the fluid any further to influence the frictional pressure gradient of the flow. The effect of the annuli pipe diameter ratio could be seen when the friction geometry parameter values for the Power law fluid without inner pipe rotation (Figure 29) was compared to cases when the inner pipe rotation was 300 rpm (Figure 30). For the cases of pipe rotation, even though the friction geometry parameter was significantly reduced, it can be deduced from Figure 30, that the maximum effect of the inner pipe rotation occurred within the annuli geometry parameter range of about 0.6 to 0.8. The same phenomenon can be seen in the comparison of the friction geometry parameter for the Herschel-Bulkley fluid at a flowrate of 14 $m^3$/hr without inner pipe rotation (Figure 31) to that which had inner pipe rotation (Figure 32). However, due to the fluid rheological parameters used in this study, the impact of the inner pipe rotation is more significant in the Power law fluid when compared to the Herschel-Bulkley fluid. The effect of inner pipe rotation on the friction geometry parameter at various annuli pipe diameter ratios for the flow of the Power law fluids at a fixed eccentricity is presented in Figure 33 and Figure 34. These figures show that the influence of inner pipe rotation is less pronounced at the lowest and highest pipe diameter ratios and in some cases, the friction geometry parameters approach the same value at those points and tend to return to the values obtained in the cases of no pipe rotation.

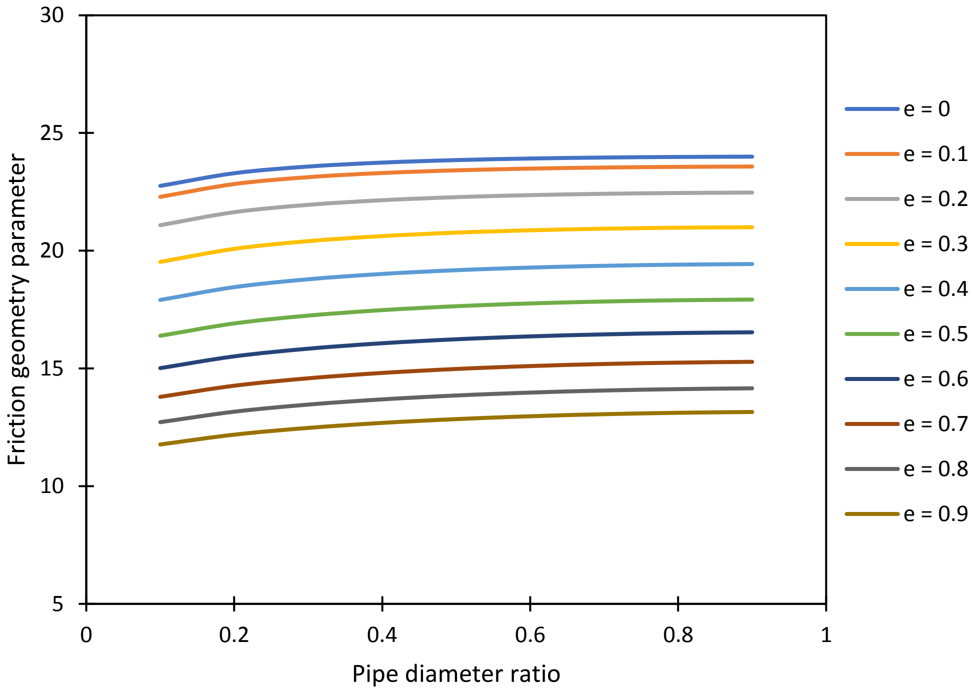


Figure 29: Friction geometry parameter for the Power law fluid (K = 0.678, n = 0.27, $\tau_o$ = 0) at 14 $m^3$/hr and 0 rpm

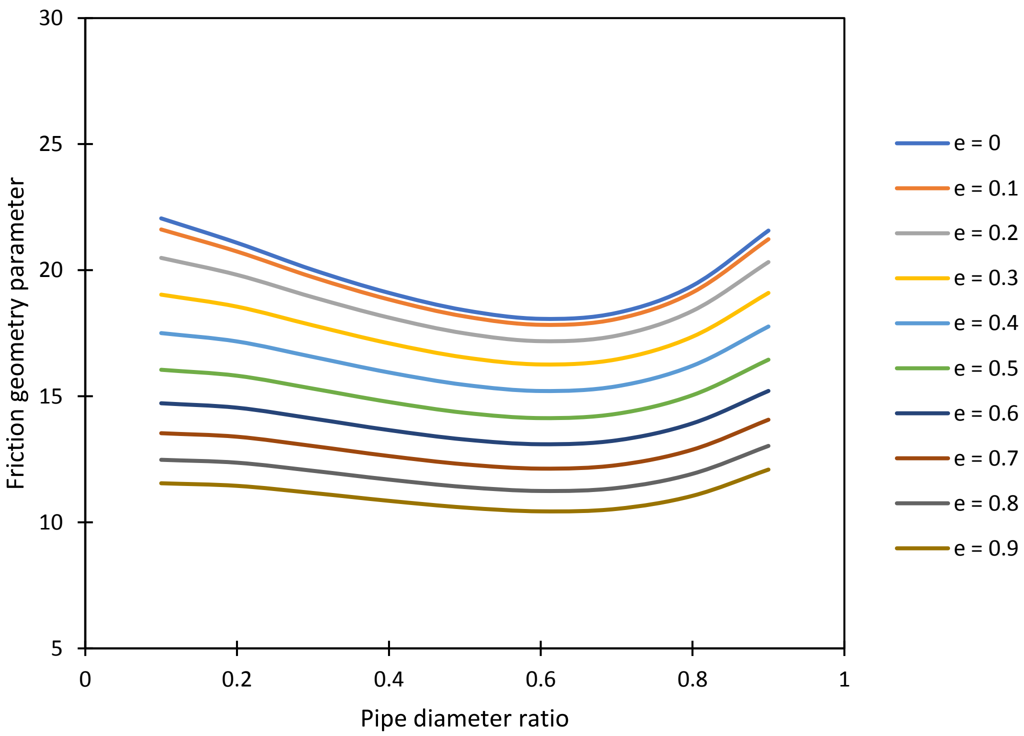


Figure 30: Friction geometry parameter for the Power law fluid (K = 0.678, n = 0.27, $\tau_o$ = 0) at 14 $m^3$/hr and 300 rpm

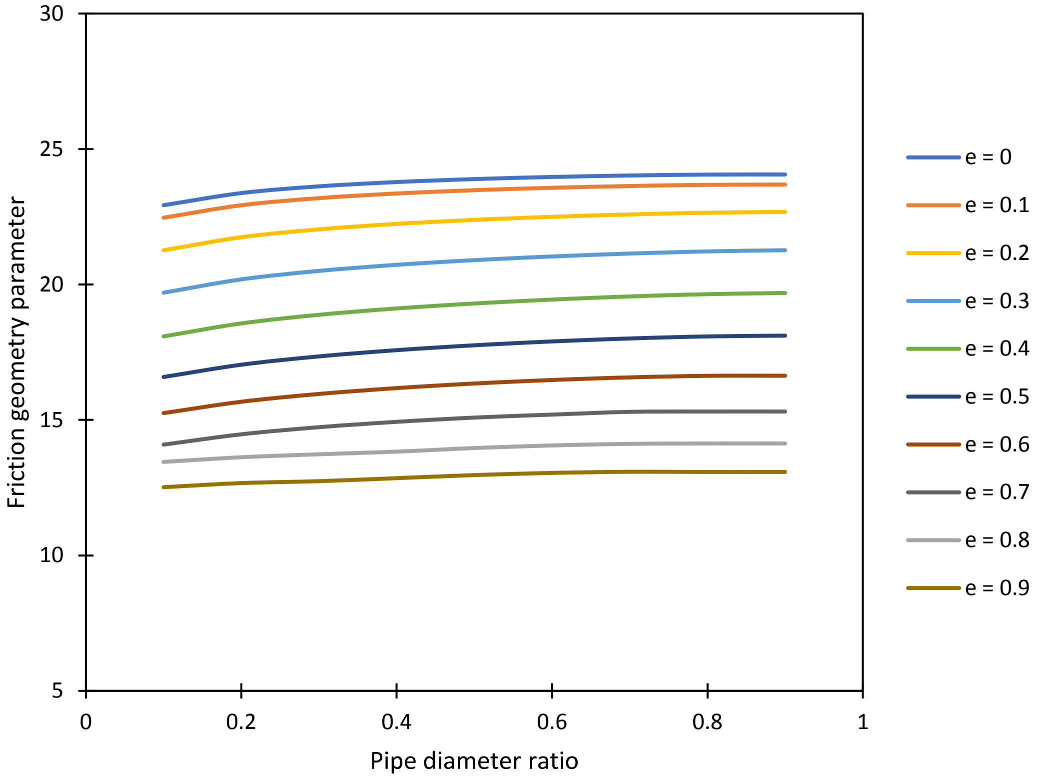


Figure 31: Friction geometry parameter for the Herschel-Bulkley fluid (K = 0.6461, n = 0.43, $\tau_o$ = 2.29) at 14 $m^3$/hr and 0 rpm

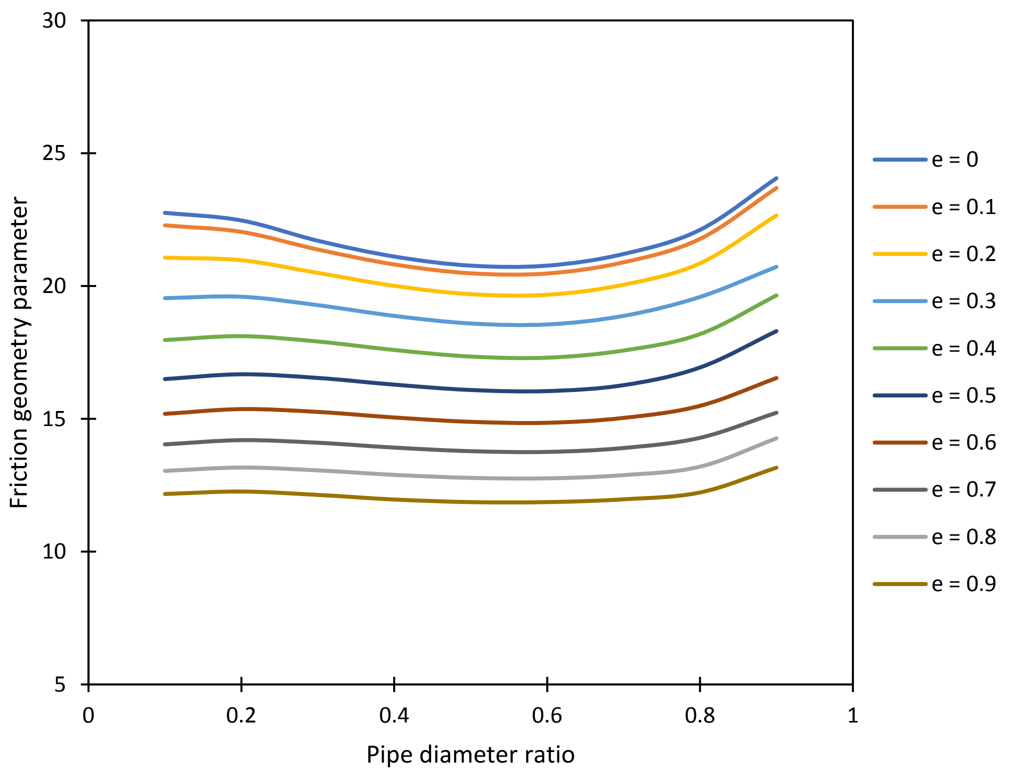


Figure 32: Friction geometry parameter for the Herschel-Bulkley fluid (K = 0.6461, n = 0.43, $\tau_o$ = 2.29) at 14 $m^3$/hr and 300 rpm

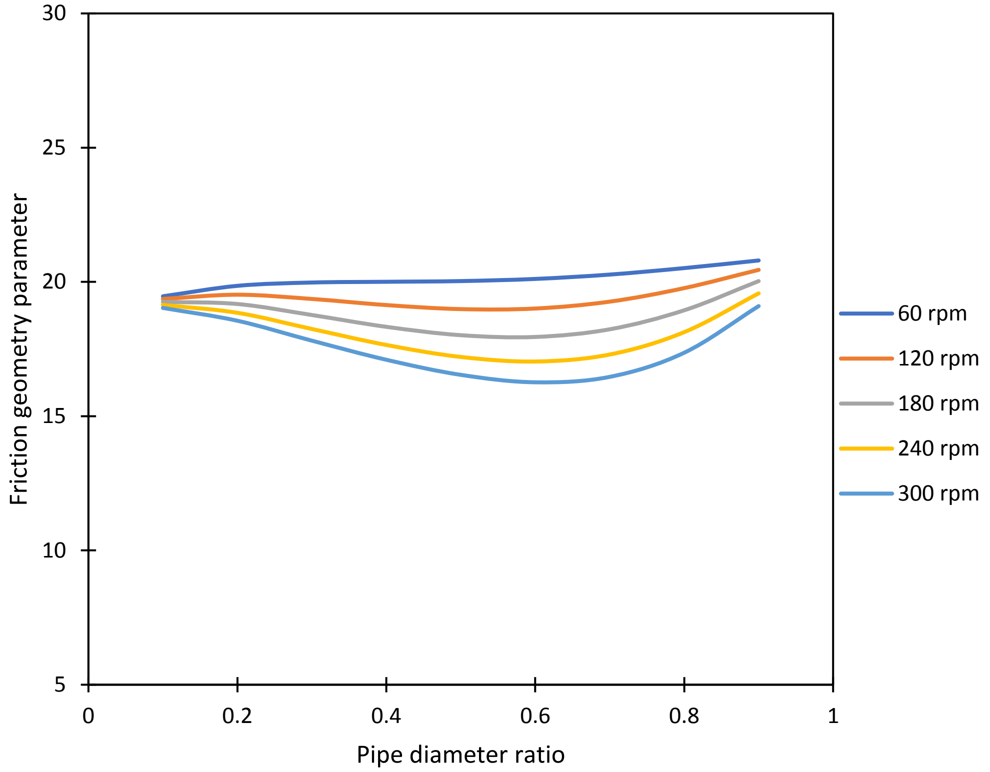


Figure 33: Effect of inner pipe rotation on the friction geometry parameter of the Power law fluid (K = 0.678, n = 0.27, $\tau_o = 0$) at 14 $m^3$/hr, in the eccentric annuli (e = 0.3) at different pipe diameter ratios

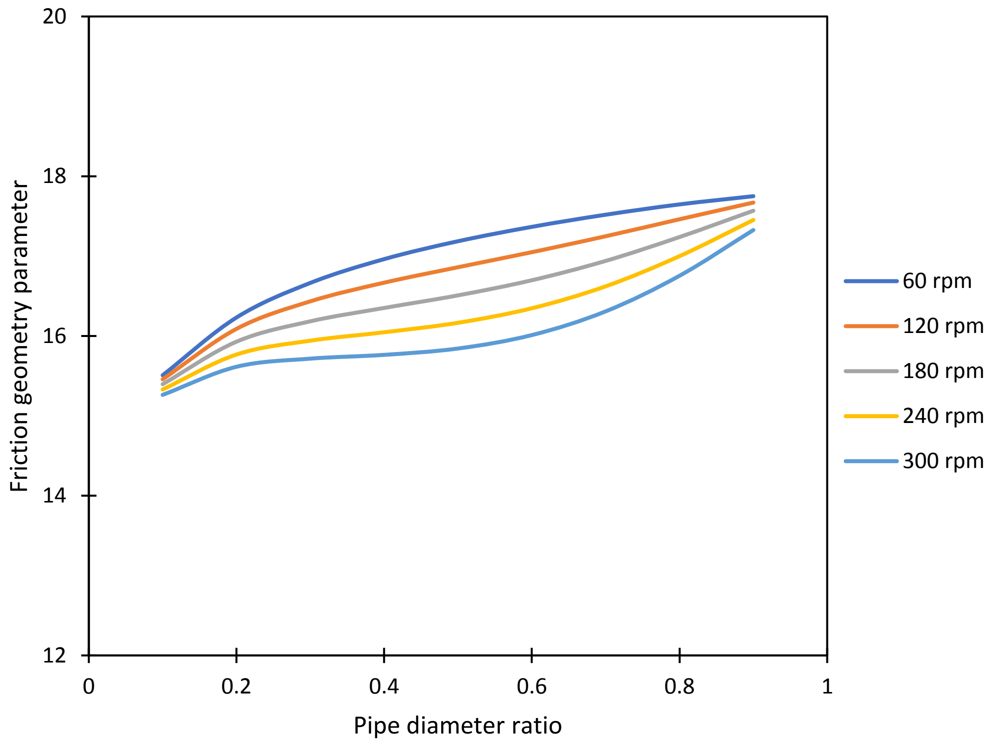


Figure 34: Effect of inner pipe rotation on the friction geometry parameter of the Power law fluid (K = 0.096, n = 0.75, $\tau_o = 0$) at 14 $m^3$/hr, in the eccentric annuli (e = 0.5) at different pipe diameter ratios

**5.5 Axial frictional pressure gradient**

Analytical calculations and numerical simulations results have showed that for the flow of non-Newtonian fluids, the friction geometry parameter and thus, the axial pressure gradient in the annuli is dependent on the combined effect of the fluid flowrate, fluid rheology, eccentricity, inner pipe rotary speed and annuli pipe diameter ratio. Figure 35 to Figure 40 display the results of the comparison of the axial pressure gradient obtained from the analytical and numerical model for different inner pipe rotation speeds, fluid flowrates and eccentricities, and for all the simulated non-Newtonian fluids. It was observed that although the increase in the inner pipe rotation led to a decrease in the frictional pressure gradient, the effect of the pipe rotation is dependent on the fluid flowrate. For instance, comparing Figure 35 and Figure 36, it can be seen that while the increase in the inner pipe rotation had an effect on the pressure gradient of the Power law fluid at the fluid flowrate of 10 $m^3$/hr, this effect is somewhat negligible at the fluid flowrate of 60 $m^3$/hr. In general, the comparison of the pressure gradient calculated using the new analytical models to that obtained using the numerical CFD models showed very good agreement with a maximum error of about 10%.

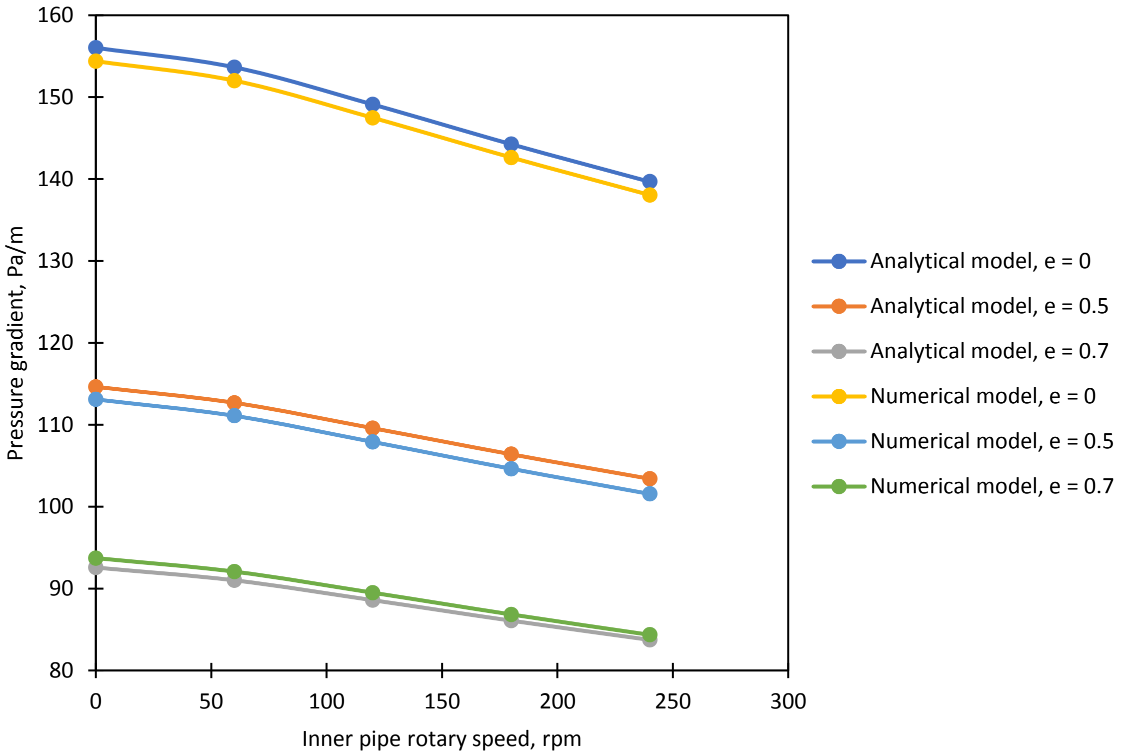


Figure 35: Axial frictional pressure gradient at different pipe rotation speeds, obtained from the analytical and numerical model for the flow of the Power law fluid ($K = 0.096$, $n = 0.75$, $\tau_o = 0$) at 10 $m^3$/hr in the concentric ($e = 0$) and eccentric ($e = 0.5$ and 0.7) annuli

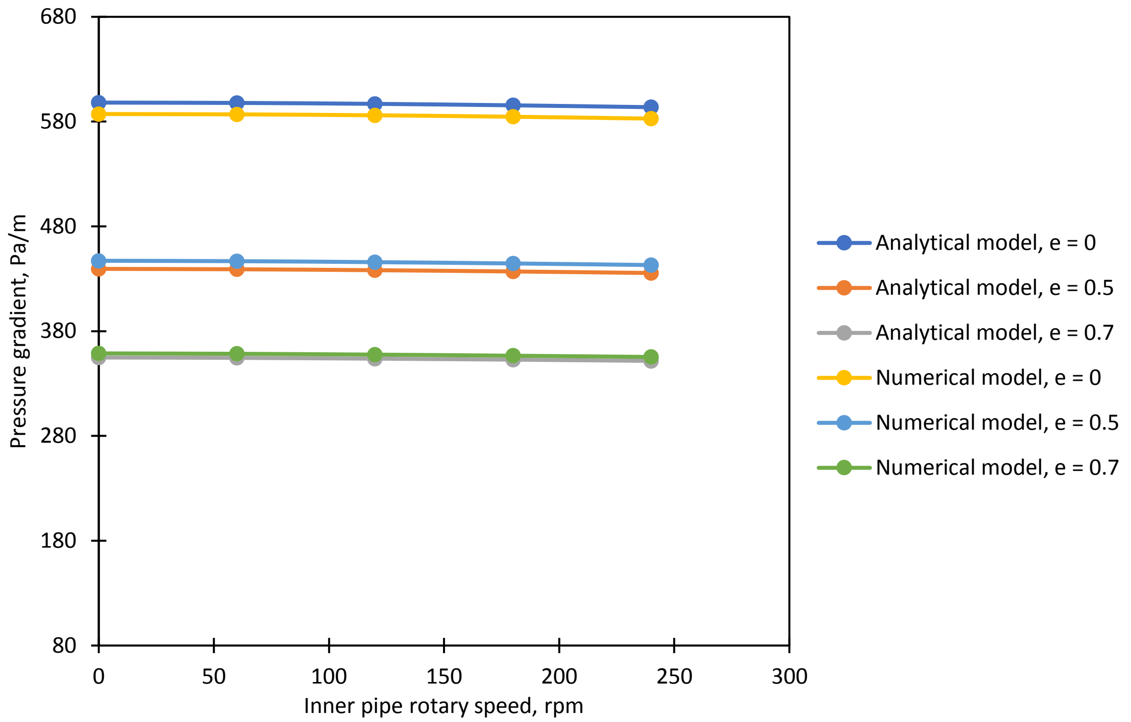


Figure 36: Axial frictional pressure gradient at different pipe rotation speeds, obtained from the analytical and numerical model for the flow of the Power law fluid (K = 0.096, n = 0.75, $\tau_o = 0$) at 60 $m^3$/hr in the concentric (e = 0) and eccentric (e = 0.5 and 0.7) annuli

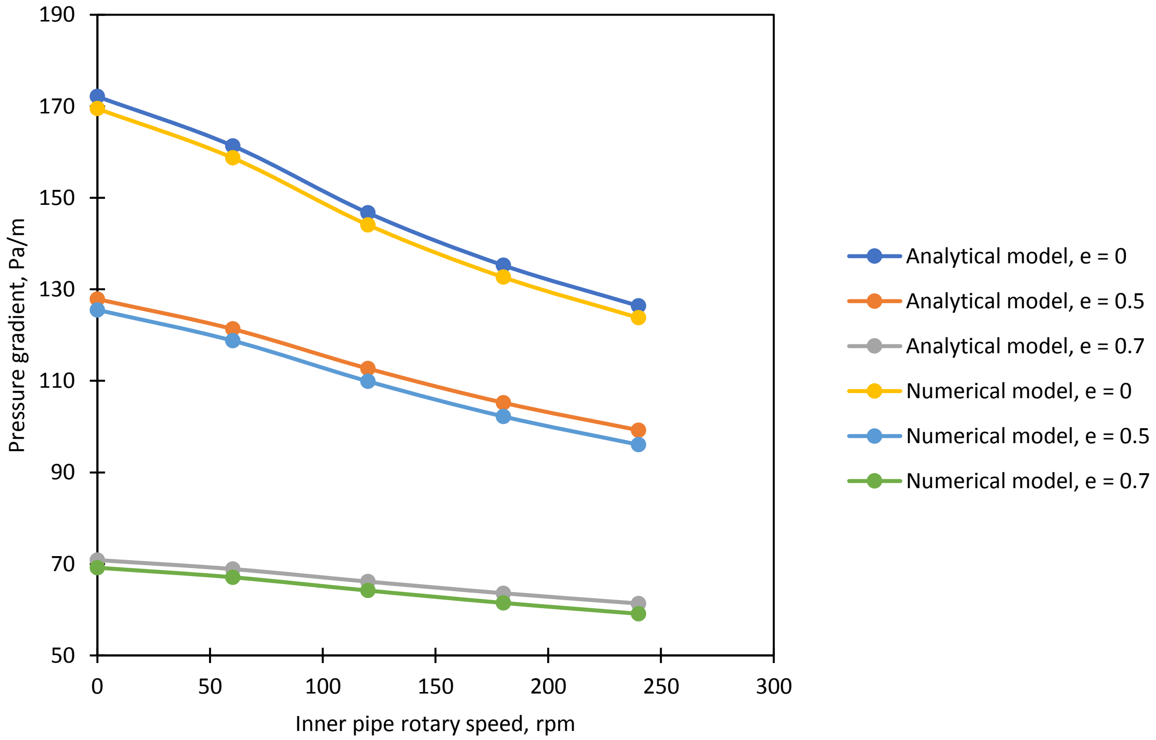


Figure 37: Axial frictional pressure gradient at different pipe rotation speeds, obtained from the analytical and numerical model for the flow of the Power law fluid (K = 0. 678, n = 0.27, $\tau_o = 0$) at 10 $m^3$/hr in the concentric (e = 0) and eccentric (e = 0.5 and 0.7) annuli

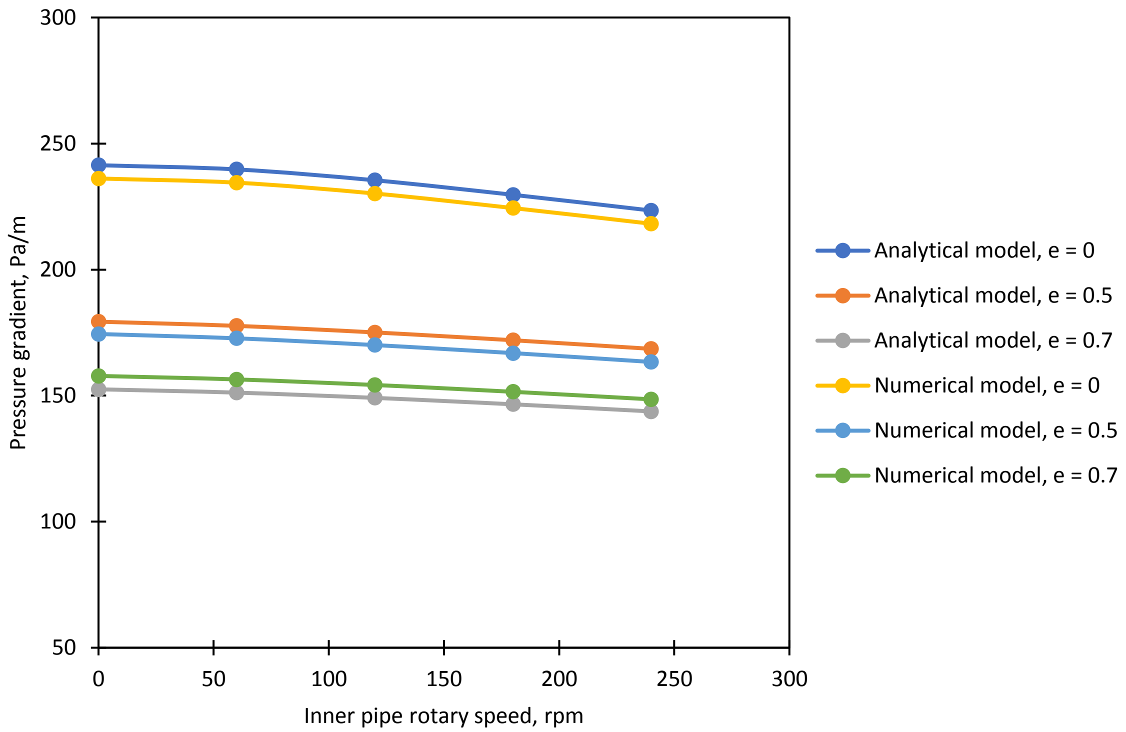


Figure 38: Axial frictional pressure gradient at different pipe rotation speeds, obtained from the analytical and numerical model for the flow of the Power law fluid (K = 0. 678, n = 0.27, $\tau_o$ = 0) at 35 m$^3$/hr in the concentric (e = 0) and eccentric (e = 0.5 and 0.7) annuli

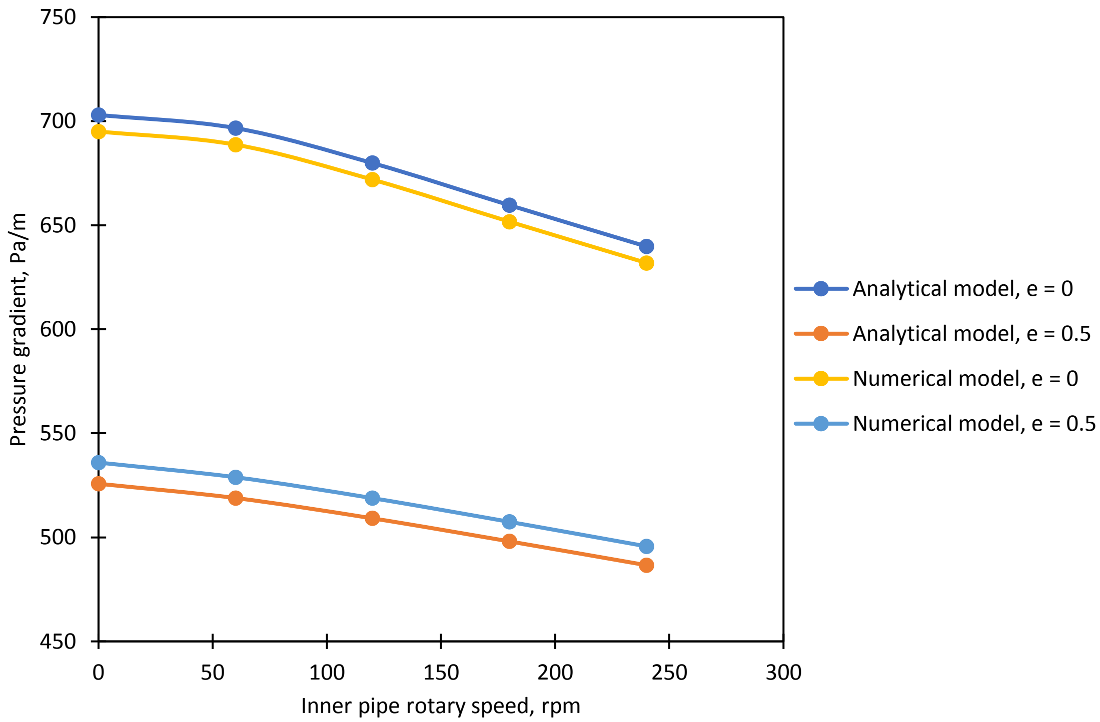


Figure 39: Axial frictional pressure gradient at different pipe rotation speeds, obtained from the analytical and numerical model for the flow of the Herschel-Bulkley fluid (K = 0.6461, n = 0.43, $\tau_o$ = 2.29) at 30 m$^3$/hr in the concentric (e = 0) and eccentric (e = 0.5) annuli

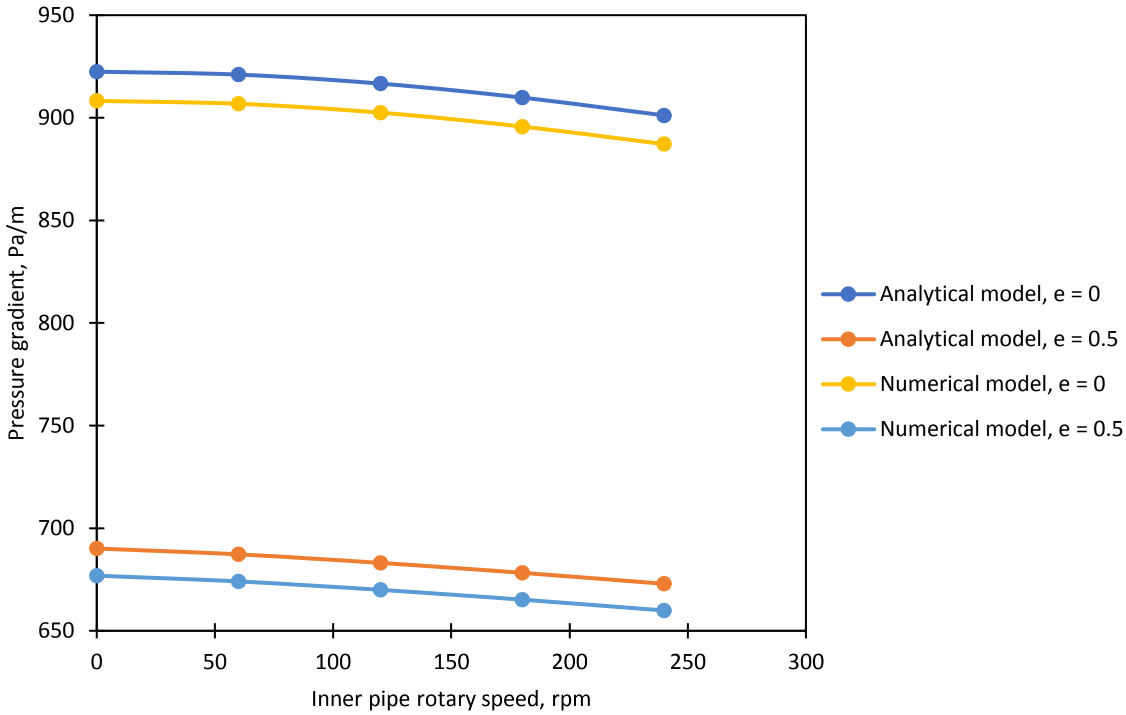


Figure 40: Axial frictional pressure gradient at different pipe rotation speeds, obtained from the analytical and numerical model for the flow of the Herschel-Bulkley fluid (K = 0.6461, n = 0.43, $\tau_o$ = 2.29) at 70 $m^3$/hr in the concentric (e = 0) and eccentric (e = 0.5) annuli

### 5.6 Rotational versus orbital motion of the inner pipe

Analysis of the results presented has shown that when the annuli flow is fully developed and the fluid flowrate is held constant, the increase in the inner pipe rotation leads to a decrease in the pressure gradient for the shear thinning non-Newtonian fluids. Although, the magnitude of this effect is highly dependent on the fluid rheological properties, inner pipe rotation and the annuli eccentricity, it is also dependent on whether the inner pipe is exhibiting a rotational or an orbital motion. For instance, Erge et al (2014b) pointed out that there are several drillstring motion patterns that may be expected to form when the drillpipe is rotating and at high rotary speeds, an irregular motion of the drillstring of the drillstring can occur. It is important to point out that the new analytical and numerical models developed in this study is only valid when the pipe is moving in a rotational motion and cannot be applied directly to investigate the effect of rotation on the fluid dynamics when the inner pipe is moving in an orbital motion. If the inner pipe is moving in an orbital motion, depending on the axial deflection or sag of the inner pipe, the eccentricity of the annuli changes constantly as the pipe is moving and thus the distance between the inner pipe wall and the outer pipe wall across the circumference of the annuli would not be constant with time at any given location (Figure 41).

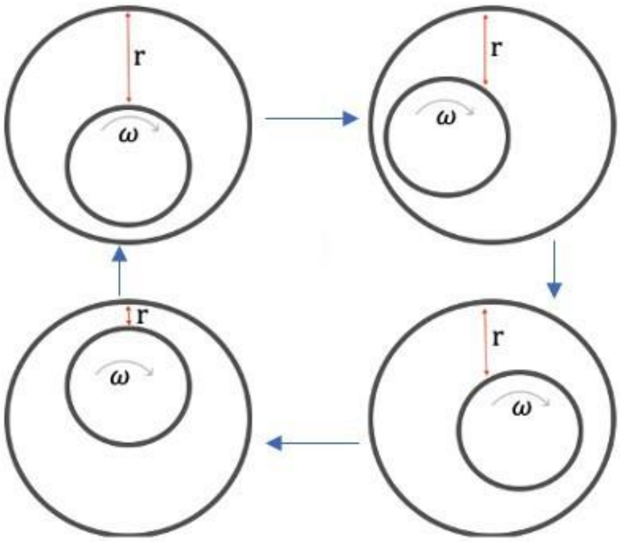


Figure 41: Change in eccentricity and position of inner pipe in the annuli due to orbital motion

The changes in eccentricity and the radial position caused by the inner pipe orbital motion leads to a transient distribution of the velocity fields and the local fluid properties in the annuli. Thus, a steady-state fully developed flow cannot be assumed as the fluid velocity distribution in the annuli is transient. This phenomenon will lead to a situation where the axial pressure gradient of the flow can either be increased or decreased with an increase in the inner pipe rotary speed and the setup of numerical CFD simulations to account for this transient effect while obtaining solutions for the transient governing equations for the fluid flow is highly complex. However, an experimental study can be performed to investigate the effect of the orbital motion of the inner pipe on the annuli flow dynamics and hydraulics and obtain a correction factor or parameters that can be applied to modify the analytical friction factor models to account for this effect.

## 6.0 Conclusions

New analytical and numerical models were developed to analyse the simultaneous effect of eccentricity and inner pipe rotation on the fluid dynamics and pressure gradient for the flow of Newtonian and non-Newtonian fluids through the annuli. The debate about the hydraulics of helical flow of fluids through the concentric and eccentric annuli was addressed and analytical and numerical CFD models were developed to predict the friction geometry parameter for the flow of both Newtonian and non-Newtonian fluids through the concentric and eccentric annuli with and without inner pipe rotation. These suggested mathematical models showed good agreement when compared to models published in literature and produced a maximum error of about ±7%. Numerical CFD simulations were performed using the finite volume technique to obtain axial and tangential velocity and viscosity fields to evaluate the axial pressure gradient for helical flow of both Newtonian and non-Newtonian fluids in the annuli. Furthermore, new generalised Reynolds number equations valid for Newtonian, Power law, Bingham plastic and Herschel-Bulkley fluids were derived and presented. The results of the predicted frictional pressure gradient for fluid flow in concentric and eccentric annuli, with or without inner pipe rotation, obtained using the analytical and numerical models were compared to generate a maximum error of about 10%.

The following conclusions were drawn from this study:

1. The friction geometry parameter for non-Newtonian fluid flow through the annuli, unlike Newtonian flow, is dependent on the rheological properties of the fluid, the fluid flowrate, inner pipe rotary speed and the annuli geometry.

2. In order to determine the friction factor and the consequent frictional pressure gradient in the annuli with or without inner pipe rotation for the flow of non-Newtonian fluids, the rheological properties along with the other important parameters of the flow have to be taken into account. Thus, the methods developed for the

flow of Newtonian fluids in the annuli cannot be applied to perform accurate predictions of the annuli pressure losses for the axial or helical flow of non-Newtonian fluids.

3. For a fully developed laminar flow of non-Newtonian shear thinning fluids, if the fluid flowrate is constant, the increase in the inner pipe rotation leads to a decrease in the axial frictional pressure gradient when the pipe is rotating on its axis. However, if the inner pipe is rotating in an orbital motion, the frictional pressure gradient can either increase or decrease depending on the flow dynamics and annuli geometry.

4. When the fluid flowrate is held constant, while inner pipe rotation has a little or no effect on the axial velocity distribution in the annuli for the flow of Newtonian fluids, the increase in inner pipe rotation increases the axial velocity fields in the region of lower flow in the eccentric annuli for shear thinning non-Newtonian fluids. However, there is little or no effect of inner pipe rotation on the velocity distribution in the concentric annuli.

5. An increase in eccentricity generally leads to a corresponding decrease in the frictional pressure losses in the annuli for both single-phase Newtonian and shear thinning non-Newtonian fluids.

6. For the helical flow of non-Newtonian fluids in the annuli, the rate at which the inner pipe rotation influences the axial and tangential velocity field distribution, and the pressure gradient is dependent on the rheological parameters of the fluid

7. The effect of inner pipe rotation on the frictional pressure gradient for annuli flow of non-Newtonian fluid is dependent on the fluid flowrate. As the fluid flowrate increases the impact of the inner pipe rotation on the fluid hydraulics decreases.

8. An increase in eccentricity can influence the viscosity profile of non-Newtonian fluids in the annuli. However, the increase in the inner pipe rotation significantly decreases the annuli fluid viscosity, especially in the smallest radial gap regions of the eccentric annuli.

9. A systematic experimental study is required to investigate the difference between the effect of the inner pipe rotational and orbital motion on the fluid dynamics and hydraulics of generalised fluid flow through the concentric and eccentric annuli.

**Data availability**

The datasets generated and/or analysed during the current study are available from the corresponding author upon request.

**Acknowledgement**

The authors are grateful to the School of Engineering at Robert Gordon University for facilitating and supporting this research work.

**Conflict of interest**

The authors declare that there is no conflict of interest.

## Nomenclature

| | | |
|---|---|---|
| $A$ | = | Cross-sectional area |
| $d_e$ | = | Distance between the centre of the outer pipe and the inner pipe |
| $d_1, d_2$ | = | Diameters of the inner and outer pipe |
| $D_h$ | = | Hydraulic diameter |
| $\partial P/\partial L, \partial P/\partial z$ | = | Pressure gradient |
| $e$ | = | Wellbore eccentricity |
| $f$ | = | Friction factor |
| $F_\pi$ | = | Friction geometry parameter |
| $\mathbf{g}$ | = | Gravitational acceleration vector |
| $K$ | = | Consistency index |
| $L$ | = | Length |
| $n$ | = | Flow behaviour index |
| $\mathbf{n}$ | = | Normal vector |
| $n_x, n_y$ | = | Axial and tangential component of the normal vector |
| $P$ | = | Pressure |
| $Q$ | = | Volumetric flowrate |
| $r_1$ | = | Radius of the inner pipe |
| $r_2^e$ | = | Distance between the centre of the inner pipe and the outer pipe wall at a given angular position |
| $Re$ | = | Reynolds number |
| $\mathbf{t}$ | = | Tangent vector |
| $V$ | = | Volume |
| $V_a$ | = | Average fluid velocity |
| $\mathbf{v}$ | = | Velocity vector |
| $v_r, v_\theta, v_z$ | = | Velocity in the cylindrical coordinate system |
| $w$ | = | Weight of interpolation function |
| $\in$ | = | Consistency index |
| $\rho$ | = | Density |
| $\tau_\in$ | = | Yield stress |
| $\mu$ | = | Viscosity |
| $\omega$ | = | Angular velocity |
| $\omega_{max}$ | = | Maximum angular velocity at the drillpipe wall |
| $\gamma$ | = | Shear rate |

**Subscripts**

| | | |
|---|---|---|
| $a$ | = | Apparent |
| $aw$ | = | Apparent wall |
| $CV$ | = | Control volume |
| $CS$ | = | Control surface |
| $f$ | = | Face |
| $Gen$ | = | Generalised |
| $i$ | = | Index |
| $o$ | = | True yield |
| $p$ | = | Plastic |
| $v$ | = | Vertex |
| $w$ | = | True wall |
| $x, y$ | = | Cartesian coordinate axes |
| $y$ | = | Bingham yield |
| $\theta, r, z$ | = | Cylindrical coordinates |

# References


Ahmed, R.M., Enfis, M.S., El Kheir, H.M., Laget, M., Saasen, A., 2010. The effect of drillstring rotation on equivalent circulation density: Modeling and analysis of field measurements, in: SPE Annual Technical Conference and Exhibition. Society of Petroleum Engineers. https://doi.org/10.2118/135587-MS

Ahmed, R.M., Miska, S.Z., 2008. Experimental study and modeling of yield power-law fluid flow in annuli with drillpipe rotation, in: IADC/SPE Drilling Conference. Society of Petroleum Engineers. https://doi.org/10.2118/112604-MS

Bicalho, I.C., dos Santos, D.B.L., Ataíde, C.H., Duarte, C.R., 2016. Fluid-dynamic behavior of flow in partially obstructed concentric and eccentric annuli with orbital motion. J. Pet. Sci. Eng. 137, 202–213. https://doi.org/10.1016/j.petrol.2015.11.029

Bui, B.., 2012. Modeling the effect of pipe rotation on pressure loss through tool joint, in: All Days. SPE. https://doi.org/10.2118/157982-MS

Busch, A., Johansen, S.T., 2020. Cuttings transport: On the effect of drill pipe rotation and lateral motion on the cuttings bed. J. Pet. Sci. Eng. 191. https://doi.org/10.1016/j.petrol.2020.107136

Caetano, E.F., Shoham, O., Brill, J.P., 1992. Upward vertical two-phase flow through an annulus—Part I: Single-phase factor, Taylor bubble rise velocity, and flow pattern prediction. J. Energy Resour. Technol. 114. https://doi.org/10.1115/1.2905917

Diamante, L.M., Lan, T., 2014. Absolute viscosities of vegetable oils at different temperatures and shear rate range of 64.5 to 4835 s-1. J. Food Process. 2014, 1–6. https://doi.org/10.1155/2014/234583

Dokhani, V., Ma, Y., Li, Z., Geng, T., Yu, M., 2020. Effects of drill string eccentricity on frictional pressure losses in annuli. J. Pet. Sci. Eng. 187. https://doi.org/10.1016/j.petrol.2019.106853

Duan, M., Miska, S.Z., Yu, M., Takach, N.E., Ahmed, R.M., Hallman, J.H., 2008. The effect of drillpipe rotation on pressure losses and fluid velocity profile in foam drilling, in: All Days. SPE. https://doi.org/10.2118/114185-MS

Erge, O., Ozbayoglu, E.M., Miska, S.Z., Yu, M., Takach, N., Saasen, A., Oljeselskap, D.N., May, R., 2014a. The effects of drillstring eccentricity, rotation and buckling configurations on annular frictional pressure losses while circulating yield power law fluids, in: All Days. SPE. https://doi.org/10.2118/167950-MS

Erge, O., Ozbayoglu, M.E., Miska, S.Z., Yu, M., Takach, N., Saasen, A., May, R., 2014b. Effect of drillstring deflection and rotary speed on annular frictional pressure losses. J. Energy Resour. Technol. 136. https://doi.org/10.1115/1.4027565

Erge, O., van Oort, E., 2020. Modeling cuttings transport and annular pack-off using local fluid velocities with the effects of drillstring rotation and eccentricity, in: IADC/SPE International Drilling Conference and Exhibition. Society of Petroleum Engineers. https://doi.org/10.2118/199587-MS

Escudier, M.P., Oliveira, P.J., Pinho, F.T., 2002. Fully developed laminar flow of purely viscous non-Newtonian liquids through annuli, including the effects of eccentricity and inner-cylinder rotation. Int. J. Heat Fluid Flow 23. https://doi.org/10.1016/S0142-727X(01)00135-7

Fan, J., Wang, X., Han, S., Yu, Z., 2009. A novel approach to modeling and simulating of underbalanced drilling process in oil and gas wells. https://doi.org/10.1007/978-3-642-03664-4_45

Ferroudji, H., Hadjadj, A., Rahman, M.A., Hassan, I., Ofei, T.N., Haddad, A., 2021. The impact of orbital motion of drill pipe on pressure drop of non-Newtonian fluids in eccentric annulus. J. Adv. Res. Fluid Mech. Therm. Sci. 65, 94–108.

Haciislamoglu, M., Langlinais, J., 1990. Non-Newtonian flow in eccentric annuli. J. Energy Resour. Technol. 112. https://doi.org/10.1115/1.2905753

Hai-qiao, Z., Ji-zhou, W., 1994. Analytical solutions of the helical flow of non newtonian fluid in eccentric annular space. Appl. Math. Mech. 15. https://doi.org/10.1007/BF02451614

Hasan, A.R., Kabir, C.S., 1992. Two-phase flow in vertical and inclined annuli. Int. J. Multiph. Flow 18. https://doi.org/10.1016/0301-9322(92)90089-Y

Hemphill, T., 2015. Advances in the calculation of circulating pressure drop with and without drillpipe rotation, in: Day 1 Tue, March 17, 2015. SPE. https://doi.org/10.2118/173054-MS

Huque, M.M., Imtiaz, S., Zendehboudi, S., Butt, S., Rahman, M.A., Maheshwari, P., 2020. Experimental study of cuttings transport with non-Newtonian fluid in an inclined well using visualization and ERT techniques, in: Day 2 Tue, October 27, 2020. SPE. https://doi.org/10.2118/201709-MS

Ibarra, R., Nossen, J., Tutkun, M., 2019. Two-phase gas-liquid flow in concentric and fully eccentric annuli. Part II: Model development, flow regime transition algorithm and pressure gradient. Chem. Eng. Sci. 203. https://doi.org/10.1016/j.ces.2019.02.021

Iyoho, A.W., Azar, J.J., 1981. An accurate slot-flow model for non-Newtonian fluid flow through eccentric annuli. Soc. Pet. Eng. J. 21. https://doi.org/10.2118/9447-PA

Kelessidis, V.C., Dukler, A.E., 1989. Modeling flow pattern transitions for upward gas-liquid flow in vertical concentric and eccentric annuli. Int. J. Multiph. Flow 15. https://doi.org/10.1016/0301-9322(89)90069-4

Kelessidis, V.C., Maglione, R., Tsamantaki, C., Aspirtakis, Y., 2006. Optimal determination of rheological parameters for Herschel–Bulkley drilling fluids and impact on pressure drop, velocity profiles and penetration rates during drilling. J. Pet. Sci. Eng. 53. https://doi.org/10.1016/j.petrol.2006.06.004

Lage, A.C.V.M., Time, R.W., 2002. An experimental and theoretical investigation of upward two-phase flow in annuli. SPE J. 7. https://doi.org/10.2118/79512-PA

Luo, Y., Peden, J.M., 1990. Flow of non-Newtonian fluids through eccentric annuli. SPE Prod. Eng. 5. https://doi.org/10.2118/16692-PA

McCann, R.C., Quigley, M.S., Zamora, M., Slater, K.S., 1995. Effects of high-speed pipe rotation on pressures in narrow annuli. SPE Drill. Complet. 10. https://doi.org/10.2118/26343-PA

Metin, C.O., Ozbayoglu, M.E., 2009. Friction factor determination for horizontal two-phase flow through fully eccentric annuli. Pet. Sci. Technol. 27. https://doi.org/10.1080/10916460802686178

Nouri, J.M., Whitelaw, J.H., 1997. Flow of Newtonian and non-Newtonian fluids in an eccentric annulus with rotation of the inner cylinder. Int. J. Heat Fluid Flow 18. https://doi.org/10.1016/S0142-727X(96)00086-0

Omurlu, C., Ozbayoglu, M.E., 2006. Friction factors for two-phase fluids for eccentric annuli in CT applications, in: All Days. SPE. https://doi.org/10.2118/100145-MS

Ooms, G., Burgerscentrum, J.M., Kampman-Reinhartz, B.E., 1999. Influence of drillpipe rotation and eccentricity on pressure drop over borehole during drilling, in: SPE Annual Technical Conference and Exhibition. Society of Petroleum Engineers. https://doi.org/10.2118/56638-MS

Ozbayoglu, M.E., Sorgun, M., 2009. Frictional pressure loss estimation of non-Newtonian fluids in realistic annulus with pipe rotation, in: Canadian International Petroleum Conference. Petroleum Society of Canada. https://doi.org/10.2118/2009-042

Peden, J.M., Ford, J.T., Oyeneyin, M.B., 1990. Comprehensive experimental investigation of drilled cuttings transport in Inclined wells including the effects of rotation and eccentricity, in: European Petroleum Conference. Society of Petroleum Engineers. https://doi.org/10.2118/20925-MS

Pereira, F.A.R., Barrozo, M.A.S., Ataíde, C.H., 2007. CFD predictions of drilling fluid velocity and pressure profiles in laminar helical flow. Brazilian J. Chem. Eng. 24. https://doi.org/10.1590/S0104-66322007000400011

Pilehvari, A., Serth, R., 2009. Generalized hydraulic calculation method for axial flow of non-Newtonian fluids in eccentric annuli. SPE Drill. Complet. 24, 553–563. https://doi.org/10.2118/111514-PA

Pipe, C.J., Majmudar, T.S., McKinley, G.H., 2008. High shear rate viscometry. Rheol. Acta 47. https://doi.org/10.1007/s00397-008-0268-1

Podryabinkin, E., Rudyak, V., Gavrilov, A., May, R., 2013. Detailed modeling of drilling fluid flow in a wellbore annulus while drilling, in: Polar and Arctic Sciences and Technology; Offshore Geotechnics; Petroleum Technology Symposium. ASME, Nantes, France, pp. 1–10.

Rojas, S., Ahmed, R., Elgaddafi, R., George, M., 2017. Flow of power-law fluid in a partially blocked eccentric annulus. J. Pet. Sci. Eng. 157, 617–630. https://doi.org/10.1016/j.petrol.2017.07.060

Saasen, A., 2014. Annular frictional pressure losses during drilling—Predicting the effect of drillstring rotation. J. Energy Resour. Technol. 136. https://doi.org/10.1115/1.4026205

Salubi, V., Mahon, R., Oluyemi, G., Oyeneyin, B., 2022. Effect of two-phase gas-liquid flow patterns on cuttings transport efficiency. J. Pet. Sci. Eng. 208. https://doi.org/10.1016/j.petrol.2021.109281

Sanchez, R.A., Azar, J.J., Bassal, A.A., Martins, A.L., 1999. Effect of drillpipe rotation on hole cleaning during directional-well drilling. SPE J. 4. https://doi.org/10.2118/56406-PA

Sayindla, S., Lund, B., Ytrehus, J.D., Saasen, A., 2017. Hole-cleaning performance comparison of oil-based and water-based drilling fluids. J. Pet. Sci. Eng. 159, 49–57. https://doi.org/10.1016/j.petrol.2017.08.069

Silva, M.A., Shah, S.N., 2000. Friction pressure correlations of Newtonian and non-Newtonian fluids through concentric and eccentric annuli, in: All Days. SPE. https://doi.org/10.2118/60720-MS

Sun, X., Wang, K., Yan, T., Shao, S., Jiao, J., 2014. Effect of drillpipe rotation on cuttings transport using computational fluid dynamics (CFD) in complex structure wells. J. Pet. Explor. Prod. Technol. 4. https://doi.org/10.1007/s13202-014-0118-x

Sunthankar, A.A., Kuru, E., Miska, S., Kamp, A., 2003. New developments in aerated mud hydraulics for drilling in inclined wells. SPE Drill. Complet. 18. https://doi.org/10.2118/83638-PA

Tang, M., Ahmed, R., He, S., 2016. Modeling of yield-power-law fluid flow in a partially blocked concentric annulus. J. Nat. Gas Sci. Eng. 35, 555–566. https://doi.org/10.1016/j.jngse.2016.09.001

Tong, T.A., Yu, M., Ozbayoglu, E., Takach, N., 2020. Numerical simulation of non-Newtonian fluid flow in partially blocked eccentric annuli. J. Pet. Sci. Eng. 193, 107368. https://doi.org/10.1016/j.petrol.2020.107368

Uner, D., Ozgen, G., Tosun, I., Ozgen, C., Tosun, I., 1988. An approximate solution for non-newtonian flow in eccentric annuli. Ind. Eng. Chem. Res. 27, 698–701. https://doi.org/10.1021/ie00076a028

Vieira Neto, J.L., Martins, A.L., Ataíde, C.H., Barrozo, M.A.S., 2014. The effect of the inner cylinder rotation on the fluid dynamics of non-Newtonian fluids in concentric and eccentric annuli. Brazilian J. Chem. Eng.

31. https://doi.org/10.1590/0104-6632.20140314s00002871
Wei, X., Miska, S.Z., Takach, N.E., Bern, P., Kenny, P., 1998. The effect of drillpipe rotation on annular frictional pressure loss. J. Energy Resour. Technol. 120, 61–66. https://doi.org/10.1115/1.2795011

## Appendix A

Concentric annulus:

$$f = \frac{16}{Re} \frac{(1-K_a)^2}{\left[\frac{1-K_a{}^4}{1-K_a{}^2} - \frac{1-K_a{}^2}{\ln(1/K_a)}\right]} \quad \text{Eq. (A.1)}$$

where, $K_a = d_1/d_2$

Eccentric annulus:

$$f = \frac{1}{Re} \frac{4(1-K_a)^2\left(1-K_a{}^2\right)}{\emptyset \sinh^4\eta_o} \quad \text{Eq. (A.2)}$$

$$\cosh\eta_i = \frac{K_a(1+e^2)+(1-e^2)}{2K_a e} \quad \text{Eq. (A.3)}$$

$$\cosh\eta_o = \frac{K_a(1-e^2)+(1+e^2)}{2e} \quad \text{Eq. (A.4)}$$

$$\emptyset = (\coth\eta_i - \coth\eta_o)^2\left[\frac{1}{\eta_o - \eta_i} - 2\sum_{m=1}^{\infty}\frac{2m}{\exp^{(2m\eta_i)} - \exp^{(2m\eta_o)}}\right] + \frac{1}{4}\left(\frac{1}{\sinh^4\eta_o} - \frac{1}{\sinh^4\eta_i}\right) \quad \text{Eq. (A.5)}$$

## Appendix B

The correction factor R:

$$R = 1 - 0.072\frac{e}{n}\left(\frac{D_1}{D_2}\right)^{0.8454} - 1.5\, e^2\sqrt{n}\left(\frac{D_1}{D_2}\right)^{0.1852} + 0.96\, e^3\sqrt{n}\left(\frac{D_1}{D_2}\right)^{0.2527} \quad \text{Eq. (B.1)}$$

The pressure gradient in the eccentric annuli $(dP/dL)_e$ can thus be calculated from the knowledge of the pressure gradient in the concentric annuli $(dP/dL)_c$ using the following relationship:

$$\left(\frac{dP}{dL}\right)_e = R\left(\frac{dP}{dL}\right)_c \quad \text{Eq. (B.2)}$$

## Appendix C

**Derivation of the generalised Reynolds number equation**

Considering the generalised rheology model of the fluids Eq. 1, the shear stress at the wall of the annuli can be expressed as:

$$\tau_w = \tau_\epsilon + \epsilon \, \gamma_w{}^n \qquad \text{Eq. (C.1)}$$

For incompressible fully developed 2D flows of liquids with a rate-dependent viscosity, the calculation of shear rate is more complex because unlike that of Newtonian fluids the velocity profile is not parabolic. The true wall shear rate can be found using the Weissenberg-Rabinowitsch-Mooney (WRM) equation expressed for flow through a slit as (Pipe et al., 2008):

$$\gamma_w = \frac{1}{3}\gamma_{aw}\left[2 + \frac{1}{m}\right] \qquad \text{Eq. (C.2)}$$

The term $\gamma_{aw}$ represents the apparent shear rate while the constant $m$ is the gradient of the log-log plot of the shear stress against the shear rate and may be expressed as:

$$m = \frac{d\ln(\tau_w)}{d\ln(\gamma_{aw})} \qquad \text{Eq. (C.3)}$$

The constant $m$ can be determined by the differentiation (chain rule) of the logarithmic expression as follows:

$$m = \frac{d\ln(\tau_w)}{d\ln(\gamma_{aw})} = \frac{d\ln(\tau_\epsilon + \epsilon \, \gamma_{aw}{}^n)}{d\ln(\gamma_{aw})} \qquad \text{Eq. (C.4)}$$

$$m = \frac{d}{d\ln(\gamma_{aw})}\ln\left(\tau_\epsilon + \epsilon \;\, e^{n\,\ln(\gamma_{aw})}\right) \qquad \text{Eq. (C.5)}$$

$$m = \frac{n \;\epsilon\; \gamma_{aw}{}^n}{\tau_\epsilon + \epsilon\; \gamma_{aw}{}^n} \qquad \text{Eq. (C.6)}$$

The apparent shear rate at the wall of the annuli in the case of a Newtonian fluid flow can be expressed as:

$$\gamma_{aw} = \frac{12V_a}{D_h} \qquad \text{Eq. (C.7)}$$

Substituting Eq. (C.7) into Eq. (C.2) and Eq. (C.6) and simplifying the result yields the final expression for the shear rate at the wall of the annuli as:

$$\gamma_w = \left(\frac{2m+1}{3m}\right)\left(\frac{12V_a}{D_h}\right) \qquad \text{Eq. (C.8)}$$

$$m = \frac{n \in \left(\frac{12V_a}{D_h}\right)^n}{\tau_\epsilon + \in \left(\frac{12V_a}{D_h}\right)^n} \qquad \text{Eq. (C.9)}$$

Using Eq. (C.8), the shear stress at the wall of the drilling annuli yields:

$$\tau_w = \tau_\epsilon + \in \left(\frac{2m+1}{3m}\right)^n \left(\frac{12V_a}{D_h}\right)^n \qquad \text{Eq. (C.10)}$$

The relationship between the friction factor and the Reynolds number may be written as:

$$Re = \frac{24}{f} \qquad \text{Eq. (C.11)}$$

Using Eq. (C.10), the friction factor f can be expressed of the wall shear stress as:

$$f = \frac{2\tau_w}{\rho {V_a}^2} = \frac{2\left(\tau_\epsilon + \in \left(\frac{2m+1}{3m}\right)^n \left(\frac{12V_a}{D_h}\right)^n\right)}{\rho v^2} \qquad \text{Eq. (C.12)}$$

Thus, from Eq. (C.11), the Reynolds number that characterises the flow of Newtonian and non-Newtonian fluids in the annuli, $Re_{Gen}$ can be

$$Re_{Gen} = 24 \, \frac{\rho {V_a}^2}{2\left(\tau_\epsilon + \in \left(\frac{2m+1}{3m}\right)^n \left(\frac{12V_a}{D_h}\right)^n\right)} \qquad \text{Eq. (C.13)}$$

Eq. (C.13) can be simplified and expressed in the generalised form yielding Eq.4.

## Appendix D

Computational procedure for numerical model